New test of modified gravity with gravitational wave experiments

N. M. Jiménez Cruz,[1,*] Flavio C. Sánchez,[1,2,†] and Gianmassimo Tasinato[1,3,‡]
[1]*Physics Department, Swansea University, Wales SA2 8PP, United Kingdom*
[2]*Unidad Académica de Física, Universidad Autónoma de Zacatecas, Zacatecas 98060, Mexico*
[3]*Dipartimento di Fisica e Astronomia, Università di Bologna, INFN, Sezione di Bologna, viale B. Pichat 6/2, 40127 Bologna, Italy*

(Received 18 September 2025; accepted 8 January 2026; published 4 February 2026)

We propose a new strategy to probe nontensorial polarizations in the stochastic gravitational wave (GW) background. Averaging over polarization angles, we find that three-point correlations of the GW signal vanish for tensor and vector modes, while scalar modes generically leave a nonzero imprint. This property makes the GW bispectrum a distinctive and robust diagnostic of scalar polarizations predicted in theories beyond general relativity. We derive the corresponding response functions for ground-based interferometers, pulsar timing arrays, and astrometric observables, and we construct an optimal estimator together with simple Fisher forecasts for pulsar timing sensitivity. As a proof of principle, we show that second-order GWs sourced by primordial magnetogenesis can be characterized by large three-point functions. Our results demonstrate that GW three-point correlations provide a novel observational window on physics beyond general relativity.

DOI: 10.1103/wy1k-f8bn

I. INTRODUCTION

One of the most exciting opportunities offered by gravitational wave (GW) observations is the ability to test general relativity (GR) as a fundamental theory of gravity in regimes inaccessible to other experiments. See, e.g., [1–3] for comprehensive textbooks on GW physics. Many alternatives to GR predict additional degrees of freedom, which may manifest as long-range interactions or as extra polarizations in GW signals [4–6]. Such effects could be revealed either in signals from compact-binary mergers or in the stochastic gravitational wave background (SGWB; see, e.g., [7–9] for reviews). The latter possibility is especially timely, given the recent evidence for a SGWB from pulsar timing arrays (PTAs) [10–13].

By combining data from multiple GW detectors, it is, in principle, possible to separate the contributions of different polarization states to the SGWB. This idea has been extensively explored for ground-based interferometers, where signals can be linearly combined in the time domain to form so-called null streams, thereby isolating specific contributions from nonstandard polarization modes: see, e.g., [14] for recent experimental bounds on extra GW polarizations. In the context of PTAs and astrometric experiments, the standard approach instead exploits the nonquadrupolar angular patterns that additional polarizations imprint on PTA overlap reduction functions. By combining timing residuals from multiple pulsars and weighting them by appropriate powers of the noise covariance matrix, we can extract possible contributions from extra polarizations (see, e.g., [15–30]). Intriguingly, recent analyses have even suggested tentative hints of possible modified-gravity effects [31–33]. Nevertheless, isolating the signatures of different polarization states remains challenging, due to both instrumental and astrophysical systematics. Imperfect knowledge of noise sources—both intrinsic to the pulsar, or "local" uncertainties such as monopolar or dipolar contributions from clock or ephemeris errors—can mimic the effects of extra polarizations. Moreover, theoretical uncertainties complicate the problem: screening mechanisms may suppress the amplitude of additional modes relative to the standard tensorial (spin-2) ones [34–36], while cosmological sources of SGWB may introduce nontrivial frequency dependencies, which further complicate attempts to disentangle among the distinct polarization contributions, when combining signals.

This motivates a natural question: is there a way to probe extra GW polarizations more directly, without relying on combinations of signals? In this work we propose a simple but powerful idea: the three-point correlation function of an isotropic and stationary SGWB provides a clean discriminator

*Contact author: nmjc1209@gmail.com
†Contact author: flavio.sanchez@fisica.uaz.edu.mx
‡Contact author: g.tasinato2208@gmail.com

of scalar (spin-0) polarizations. We show that the response of GW detectors—including ground-based interferometers, PTAs, and astrometric observatories—to the GW three-point function vanishes identically for tensor (spin-2) and vector (spin-1) modes, but is nonvanishing for scalar modes. Thus, any detection of a nonzero three-point function induced by an astrophysical or cosmological source of an isotropic SGWB would constitute an unambiguous and robust signature of scalar GW polarizations, uncontaminated by other degrees of freedom. Moreover—at least if noise sources are in good approximation Gaussian—this method can be less prone to certain types of systematic errors (e.g., related with pulsar timing uncertainties), since noise contributions do not directly contribute to the three-point function.

Our paper is organized as follows. In Sec. II, we prove that the isotropic three-point correlation function is sensitive only to GW scalar polarizations under well-defined assumptions, and we start discussing possible physical sources of three-point GW correlators. We then derive the three-point response functions of GW experiments to GW scalar polarizations. In Sec. III, we construct an optimal estimator to extract scalar contributions from GW data and present some preliminary forecasts for the sensitivity of PTA experiments. In Sec. IV, we illustrate our framework with an specific early-Universe scenario that can enhance the scalar GW three-point function to potentially observable levels. We summarize our findings in Sec. V. Throughout the paper we adopt natural units.

II. THREE-POINT FUNCTIONS AND GRAVITATIONAL WAVE EXPERIMENTS: A TEST FOR SCALAR POLARIZATIONS

A. The idea

We begin by providing an intuitive explanation of why measuring a nonvanishing three-point function of GW signals would necessarily indicate the presence of scalar GW polarizations in a stochastic SGWB background. In all our analysis, we assume the SGWB to be stationary and isotropic, but it can be characterized by non-Gaussian features. Moreover, additional GW polarizations besides Einsteinian ones might be present in the data.

In the present section we focus on a noiseless GW signal s and defer a discussion of the role of the noise to Sec. III. The GW signal is schematically expressed as the contraction

$$s = D^{ij} h_{ij}, \tag{2.1}$$

where the tensor D^{ij} encodes the geometry and response of the detector, while h_{ij} denotes the GW field. Correlating such signals and averaging over all possible GW directions we can reveal the existence of an isotropic SGWB. The GW field can be Fourier decomposed into plane waves as

$$h_{ij}(t,\mathbf{x}) = \sum_{\lambda=1}^{6} \int_{-\infty}^{\infty} df \int d^2\mathbf{n} h_\lambda(f,\mathbf{n}) \mathbf{e}_{ij}^{(\lambda)}(\mathbf{n}) e^{i2\pi f(t-\mathbf{n}\cdot\mathbf{x})}, \tag{2.2}$$

with $h_\lambda^*(f,\mathbf{n}) = h_\lambda(-f,\mathbf{n})$ ensuring that h_{ij} is real. The index λ runs over the six possible polarizations in a general metric theory of gravity: $(+,\times)$ for tensor modes; $(v1, v2)$ for vector modes; and (b,ℓ) for the scalar breathing and longitudinal modes, respectively [4–6]. In Eq. (2.2) we integrate over all possible directions of the unit vector $\mathbf{n}$, as well as over frequencies which run on the entire real line.

Introducing two orthonormal unit vectors $\boldsymbol{u}$ and $\boldsymbol{v}$ perpendicular to $\mathbf{n}$, the six polarization tensors can be expressed as

$$\mathbf{e}_{ij}^{(+)} = u_i u_j - v_i v_j, \qquad \mathbf{e}_{ij}^{(\times)} = u_i v_j + v_i u_j, \tag{2.3a}$$

$$\mathbf{e}_{ij}^{(v1)} = n_i u_j + u_i n_j, \qquad \mathbf{e}_{ij}^{(v2)} = n_i v_j + v_i n_j, \tag{2.3b}$$

$$\mathbf{e}_{ij}^{(b)} = u_i u_j + v_i v_j, \qquad \mathbf{e}_{ij}^{(\ell)} = n_i n_j. \tag{2.3c}$$

The tensors in Eqs. (2.3a)–(2.3c) correspond to spin-2, spin-1, and spin-0 polarizations, respectively, each with well-defined transformation properties under spatial rotations. Our main interest is the scalar breathing mode (b), and we focus on it in this work. We choose not to consider the longitudinal mode (ℓ) since in various Lorentz-covariant modifications of gravity such mode, if present, would correspond to a ghost degree of freedom, which would invalidate the setup and must then be excluded.[1]

An ambiguity arises from the freedom to choose the basis vectors $\boldsymbol{u}$ and $\boldsymbol{v}$. Any pair obtained by rotating through an angle ψ in the plane orthogonal to $\mathbf{n}$ defines an equally valid basis,

$$\begin{aligned} \boldsymbol{u} &\to \boldsymbol{u}' = \cos\psi \boldsymbol{u} + \sin\psi \boldsymbol{v}, \\ \boldsymbol{v} &\to \boldsymbol{v}' = -\sin\psi \boldsymbol{u} + \cos\psi \boldsymbol{v}, \end{aligned} \tag{2.4}$$

and the polarization tensors can be redefined accordingly. In fact, under this transformation, the spin-2 and spin-1 tensors rotate as

[1]Nevertheless, some care is required. Although healthy modified-gravity theories contain only one scalar degree of freedom, it sometimes manifests as a linear combination of the breathing and longitudinal modes rather than a pure breathing mode. Accordingly, we defer a detailed discussion of the longitudinal-mode detectability to future work.

$$\begin{pmatrix} \mathbf{e}^{(+)} \\ \mathbf{e}^{(\times)} \end{pmatrix} \to \begin{pmatrix} \cos 2\psi & -\sin 2\psi \\ \sin 2\psi & \cos 2\psi \end{pmatrix} \begin{pmatrix} \mathbf{e}^{(+)} \\ \mathbf{e}^{(\times)} \end{pmatrix},$$
$$\begin{pmatrix} \mathbf{e}^{(v1)} \\ \mathbf{e}^{(v2)} \end{pmatrix} \to \begin{pmatrix} \cos \psi & -\sin \psi \\ \sin \psi & \cos \psi \end{pmatrix} \begin{pmatrix} \mathbf{e}^{(v1)} \\ \mathbf{e}^{(v2)} \end{pmatrix}, \tag{2.5}$$

while the scalar-polarization tensors $\mathbf{e}^{(b)}_{ij}$ and $\mathbf{e}^{(\ell)}_{ij}$ remain invariant.

Observable quantities derived from the GW signal s should be independent of the arbitrary polarization angle ψ. As a concrete way to ensure this invariance, we average over ψ in the plane orthogonal to $\mathbf{n}$ [37].[2] This averaging has no effect on two-point functions, at least when focusing on a isotropic stochastic gravitational wave background, as we do in this work. For instance, the combination

$$\mathbf{e}^{(+)}_{ij}\mathbf{e}^{(+)}_{ij} + \mathbf{e}^{(\times)}_{ij}\mathbf{e}^{(\times)}_{ij} \tag{2.6}$$

is manifestly invariant under (2.5)—which leads to an overall factor $\cos^2 2\psi + \sin^2 2\psi = 1$—so averaging over ψ leaves it unchanged. In contrast, three-point functions involving only spin-2 and spin-1 polarizations contain terms linearly proportional to $\sin(n\psi)$ or $\cos(n\psi)$ (with n equal to the spin), which vanish upon ψ-averaging. Only three-point functions involving spin-0 (scalar) polarizations survive this procedure.[3]

Therefore, within this approach, the detection of a nonzero three-point function in measurements of an isotropic SGWB would constitute a clear signature of scalar GW polarizations. Interestingly, this method is particularly direct, as it does not require constructing weighted combinations of GW data to isolate specific polarizations in the SGWB. Moreover, being a null-type experiment, it can reveal signatures of scalar polarizations even if their amplitude is suppressed with respect to Einsteinian tensor polarizations due to screening effects (see, e.g., [34–36] for reviews).

In Secs. II C and II D, we make these considerations more concrete by explicitly computing the overlap reduction functions for three-point correlations involving scalar modes. We initially assume the following structure for the two- and three-point functions of the Fourier components of the GW modes

$$\langle h_{\lambda_1}(f_1,\mathbf{n}_1)h_{\lambda_2}(f_2,\mathbf{n}_2)\rangle = \delta(f_1+f_2)\frac{\delta^{(2)}(\mathbf{n}_1-\mathbf{n}_2)}{4\pi}P_{\lambda_1\lambda_2}(f_1), \tag{2.7}$$

$$\langle h_{\lambda_1}(f_1,\mathbf{n}_1)h_{\lambda_2}(f_2,\mathbf{n}_2)h_{\lambda_3}(f_3,\mathbf{n}_3)\rangle = \delta(f_1+f_2+f_3)\frac{\delta^{(2)}(\mathbf{n}_1-\mathbf{n}_3)}{4\pi}\frac{\delta^{(2)}(\mathbf{n}_2-\mathbf{n}_3)}{4\pi} \times B_{\lambda_1\lambda_2\lambda_3}(f_1,f_2,f_3). \tag{2.8}$$

The function $P_{\lambda_1\lambda_2}(f)$ is the power spectrum, while $B_{\lambda_1\lambda_2\lambda_3}$ is an instance of GW bispectrum.[4] The structure of Eq. (2.7) is consistent with statistical homogeneity and isotropy of the background. When writing a three-point function with the structure of (2.8)—besides imposing homogeneity and isotropy at the background level—we further assume stationarity of the GW three-point function, following [38]. This assumption, though restrictive, is well motivated physically and greatly simplifies the analytic structure, making detector-response calculations tractable. The corresponding configuration in momentum space is that of a folded triangle, whose side length is given by the (absolute value of) the frequencies f_i, and side directions are given by the vectors $\mathbf{n}_i$: in our case, two sides of the triangle are aligned and lie on the third side. In fact, the three vectors $\mathbf{n}_1$, $\mathbf{n}_2$, $\mathbf{n}_3$ point in the same direction, thanks to the structure of δ functions in Eq. (2.8), and the sum of the length of two sides is equal to the length of the third one. See Fig. 1.

Following Ref. [38], we now show that the ansatz (2.8) implies a stationary three-point function in real space. Recall that we restrict to the breathing scalar mode only. We define

$$D(\mathbf{n}) \equiv D^{ij}\mathbf{e}^{(b)}_{ij}(\mathbf{n})$$

and, by Fourier transforming, we write the three-point function of the detector signal as

$$\langle s(t_1)s(t_2)s(t_3)\rangle = \int df_1 df_2 df_3 \int d^2\mathbf{n}_1 d^2\mathbf{n}_2 d^2\mathbf{n}_3 \langle h_b(f_1,\mathbf{n}_1)h_b(f_2,\mathbf{n}_2)h_b(f_3,\mathbf{n}_3)\rangle \times D(\mathbf{n}_1)D(\mathbf{n}_2)D(\mathbf{n}_3)e^{2\pi i(f_1t_1+f_2t_2+f_3t_3)}e^{-2\pi i(\mathbf{n}_1\cdot\mathbf{x}_1+\mathbf{n}_2\cdot\mathbf{x}_2+\mathbf{n}_3\cdot\mathbf{x}_3)}. \tag{2.9}$$

[2]Such choice of averaging has not been performed in previous articles, as [38].

[3]We emphasize that in this work we focus exclusively on the isotropic contribution to the SGWB. Detector responses to three-point functions involving anisotropies—see, e.g., [39,40] for a theoretical analysis of non-Gaussianities in the anisotropic SGWB—may be nonvanishing even in gravity theories that do not propagate scalar polarizations. However, we expect the response of GW detectors to three-point functions involving tensor anisotropies to differ substantially from their response to isotropic scalar three-point functions, in close analogy with the well-known differences in detector responses to anisotropic versus isotropic two-point functions (see, e.g., [41]). A detailed study of these effects lies beyond the scope of the present work and is left for future investigation.

[4]Other possibilities can arise for the bispectrum, depending on whether GW interactions involve derivatives—more on this in the explicit setup of Sec. IV C.

FIG. 1. Representation of folded configurations for the shape of the tensor bispectrum in momentum space. The three side of triangles lie on top of each other, and the length of the biggest triangle side, corresponding here to frequency f_3, is equal to the sum of the other two sides, $f_1 + f_2$.

Substituting ansatz (2.8) and performing the integrals over the δ functions, we find

$$\langle s(t_1)s(t_2)s(t_3)\rangle = \int df_1 df_2 \int d^2\mathbf{n} B_{\bar{h}}(f_1, f_2, f_3) D^3(\hat{n}) e^{2\pi i f_1(t_1-t_3)+2\pi i f_2(t_2-t_3)} \times e^{-2\pi i \mathbf{n}\cdot(\mathbf{x}_1-\mathbf{x}_3)-2\pi i \mathbf{n}\cdot(\mathbf{x}_2-\mathbf{x}_3)}, \tag{2.10}$$

where the expression $B_s(f_1, f_2, f_3)$ denotes the bispectrum for the scalar breathing mode only[5] and recall that the frequencies in its argument are related by the condition $f_1 + f_2 + f_3 = 0$. It is now manifest that the three-point function is stationary, depending only on the time differences $t_1 - t_3$ and $t_2 - t_3$. As first discussed in [38], stationary three-point functions can evade the arguments of [42], which show that generic strain three-point functions, as in Eq. (2.10), are suppressed by decoherence effects between cosmological GW sources and detectors. In fact, we will return on this point within an explicit example that we develop in Sec. IV, showing explicitly in a concrete setup how dephasing works and how stationary signals avoid it. Hence our hypothesis, besides simplifying calculations, is physically very relevant. Before continuing to study the response functions of GW experiments to GW three-point functions, we briefly discuss possible sources for GW non-Gaussianity.

B. Sources for the GW three-point function

Non-Gaussian features in the SGWB can arise from both astrophysical and cosmological sources, independent of whether modified gravity is considered.

In the astrophysical case, the SGWB originates from the superposition of a large population of GW sources that are individually too weak to be resolved, but whose collective emission produces a measurable stochastic signal. If the sources are relatively rare and do not emit frequently, the signal exhibits characteristic "popcorn" features in the time domain, leading to non-Gaussian statistics [43–49]. Several methods have been proposed to capture such signatures, including extending likelihood analyses to incorporate non-Gaussian effects [43,46] or searching for four-point correlators [45] (which, unlike the three-point correlators discussed here, can yield nonvanishing responses to spin-2 polarizations). See [8] for a review. A related topic consists of analyzing shot noise effects from discrete unresolved sources contributing to the astrophysical background. Such contributions are known to induce anisotropies (see, e.g., [37] for a recent account), and it would be interesting to explore their implications for non-Gaussianity, since the associated Poisson statistics naturally generates nonvanishing three-point cumulants.

In the cosmological case, any nonlinearities in the generation of primordial GW can give rise to tensor non-Gaussianities. Numerous studies [39,50–52] have shown that cosmological mechanisms can produce a wide variety of non-Gaussian shapes, with amplitudes depending sensitively on the underlying scenario; see, e.g., [53] for a review. However, their detectability is severely limited: GWs propagating over cosmological distances tend to lose correlations and thereby erase most non-Gaussian signatures [42]. Possible ways to circumvent this problem include: (i) searching for indirect effects of squeezed non-Gaussianities that modulate the GW power spectrum at small scales [51], (ii) focusing on stationary non-Gaussian correlators [38] (this is the framework we adopt in this work; see Sec. II A, as well as Sec. IV for explicit examples), or (iii) studying non-Gaussianities in the anisotropies of the SGWB [39,40], which are not subject to such decorrelation effects.

We now turn to the detectability of stationary non-Gaussian features with GW experiments and their potential as probes of modified gravity.

C. A warm-up: The case of coincident ground based detectors

Before turning to the study of overlap reduction functions for pulsar timing arrays and astrometry, we consider here a special case in the context of ground-based detectors, which provides a simpler setting under certain assumptions. Our goal is to determine the response function of a triplet of coincident ground-based detectors to the GW three-point function of Eq. (2.8). To this end, we generalize the

[5]In principle, mixed bispectra involving scalar, tensor, and vector modes can also be considered. However, any nonzero measurement of such quantities would already indicate the presence of scalar polarizations. We therefore focus on purely scalar bispectra.

arguments of [54] (see also the textbook discussion in [1]). A possible explicit realistic example realizing this configuration is the Einstein Telescope detector [55], if it will be built in a configuration at a single location.

We denote by (1,2,3) the triplet of ground-based detectors. The signal measured say at detector a is given by the contraction of the GW tensor with the detector tensor,

$$s_1(t,\mathbf{x}) = h_{ij}(t,\mathbf{x}) d_1^{ij}, \tag{2.11}$$

where d_1^{ij} encodes the detector characteristics (arm directions and lengths). For ground-based interferometers it can be expressed as

$$d_1^{ij} = X_1^i X_1^j - Y_1^i Y_1^j, \tag{2.12}$$

with X_1 and Y_1 orthogonal unit vectors defining the arm directions. Consequently, $d_1^{ii} = 0$. Similar properties apply to detectors 2 and 3.

As an illustrative example, let us consider the instrument response to spin-2 and spin-0 (breathing-mode) polarizations. To start with, the two-point response functions are obtained from the signal correlations

$$\langle s_1(t_1,\mathbf{x}_1) s_2(t_2,\mathbf{x}_2)\rangle = \int df e^{2\pi f(t_1-t_2)} [\gamma_{12}^{\rm tens}(\mathbf{x}_1,\mathbf{x}_2) I_T(f) + \gamma_{12}^{\rm sc}(\mathbf{x}_1,\mathbf{x}_2) I_b(f)], \tag{2.13}$$

where $I_T(f)$ and $I_b(f)$ are the intensities associated with tensor and breathing scalar polarizations, while the overlap response functions are given by

$$\gamma_{12}^{\rm tens}(\mathbf{x}_1,\mathbf{x}_2) = \sum_{\lambda=+,\times} \frac{d_1^{ij} d_2^{kl}}{2\pi} \int_0^{2\pi} d\psi \times \int d^2\hat{n} e^{2\pi i f \mathbf{n}\cdot(\mathbf{x}_1-\mathbf{x}_2)} \mathbf{e}_{ij}^{\lambda}(\mathbf{n}) \mathbf{e}_{kl}^{\lambda}(\mathbf{n}), \tag{2.14}$$

$$\gamma_{12}^{\rm sc}(\mathbf{x}_1,\mathbf{x}_2) = \frac{d_1^{ij} d_2^{kl}}{2\pi} \int_0^{2\pi} d\psi \times \int d^2\hat{n} e^{2\pi i f \mathbf{n}\cdot(\mathbf{x}_1-\mathbf{x}_2)} \mathbf{e}^{(b)}{}_{ij}(\mathbf{n}) \mathbf{e}^{(b)}{}_{kl}(\mathbf{n}). \tag{2.15}$$

As explained in Sec. II A, we average over the polarization angle ψ [37]. For coincident detectors these expressions simplify considerably, assuming the arms are perpendicular, and the results can be written in closed form,

$$\gamma_{12}^{\rm tens} = \frac{8\pi}{5}, \qquad \gamma_{12}^{\rm sc} = \frac{4\pi}{15}. \tag{2.16}$$

In analogy, we calculate the three-point response functions, which are defined as

$$\gamma_{123}^{\rm tens}(\mathbf{x}_1,\mathbf{x}_2,\mathbf{x}_3) = \sum_{\lambda=+,\times} \frac{d_1^{ij} d_2^{kl} d_3^{mn}}{2\pi} \int_0^{2\pi} d\psi \int d^2\hat{n} e^{2\pi i f \mathbf{n}\cdot(\mathbf{x}_1-\mathbf{x}_2)} e^{2\pi i f \mathbf{n}\cdot(\mathbf{x}_1-\mathbf{x}_3)} \mathbf{e}_{ij}^{\lambda}(\mathbf{n}) \mathbf{e}_{kl}^{\lambda}(\mathbf{n}) \mathbf{e}_{mn}^{\lambda}(\mathbf{n}), \tag{2.17}$$

$$\gamma_{123}^{\rm sc}(\mathbf{x}_1,\mathbf{x}_2,\mathbf{x}_3) = \frac{d_1^{ij} d_2^{kl} d_3^{mn}}{2\pi} \int_0^{2\pi} d\psi \int d^2\hat{n} e^{2\pi i f \mathbf{n}\cdot(\mathbf{x}_1-\mathbf{x}_2)} e^{2\pi i f \mathbf{n}\cdot(\mathbf{x}_1-\mathbf{x}_3)} \mathbf{e}_{ij}^{(b)}(\mathbf{n}) \mathbf{e}_{kl}^{(b)}(\mathbf{n}) \mathbf{e}_{mn}^{(b)}(\mathbf{n}). \tag{2.18}$$

To compute these expressions, we follow the method of [54], focusing for simplicity on the idealized case of three coincident detectors ($\mathbf{x}_1 = \mathbf{x}_2 = \mathbf{x}_3$), while allowing for different arm orientations. Equations (2.17) and (2.18) can then be written as

$$\gamma_{123}^{\sigma}(\mathbf{x}_1,\mathbf{x}_2,\mathbf{x}_3) = d_1^{ij} d_2^{kl} d_3^{mn} \Gamma_{ijklmn}^{\sigma}, \tag{2.19}$$

where the superscript "σ" denotes either tensorial or scalar polarization. The tensors Γ_{ijklmn}^{σ} are symmetric under the exchanges $i \leftrightarrow j$, $k \leftrightarrow l$, $m \leftrightarrow n$, $ij \leftrightarrow kl$, $ij \leftrightarrow mn$, and $kl \leftrightarrow mn$, and are trace-free in each index pair. In the coincident-detector case, the six-index tensor can be constructed from Kronecker δ's,

$$\Gamma_{ijklmn}^{\sigma} = A_1^{\sigma}\delta_{ij}\delta_{kl}\delta_{mn} + A_2^{\sigma}(\delta_{ik}\delta_{jl}\delta_{mn} + \delta_{jk}\delta_{il}\delta_{mn} + \delta_{im}\delta_{jn}\delta_{kl} + \delta_{\rm in}\delta_{jm}\delta_{kl} + \delta_{km}\delta_{ln}\delta_{ij} + \delta_{kn}\delta_{ml}\delta_{ij}) + A_3^{\sigma}(\delta_{ik}\delta_{jm}\delta_{ln} + \delta_{im}\delta_{ln}\delta_{jk} + \delta_{il}\delta_{jm}\delta_{kn} + \delta_{ik}\delta_{jn}\delta_{lm}), \tag{2.20}$$

where A_i^{σ} $(i = 1,2,3)$ are constants to be determined. Contracting Eq. (2.19) with Eq. (2.20), and exploiting the tracelessness of d_{ij}, we obtain

$$\gamma_{123}^{\sigma} = 4A_3^{\sigma} d_1^{ij} d_{2i}{}^{k} d_{3jk}. \tag{2.21}$$

Following then step by step the approach of [54], contracting Eq. (2.20) with the coefficients of the A_i^σ and combining the results, we arrive at

$$\gamma_{123}^{\rm tens} = 0, \tag{2.22}$$

$$\gamma_{123}^{\rm sc} = \frac{159\pi^2}{284} d_1^{ij} d_{2i}{}^k d_{3jk}. \tag{2.23}$$

Hence, as anticipated in Sec. II A, while the three-point response function vanishes for tensor polarizations, it is nonzero for scalar polarizations and can therefore lead to a distinctive observational handle on such signals. It is straightforward to show that, for the same reasons, three-point correlations to vector polarizations vanish.

D. Overlap reduction functions for pulsar timing arrays and astrometry

We now compute the three-point correlators relevant for PTA and astrometry measurements, including the possibility of cross-correlating PTA and astrometry signals. Interestingly, the resulting overlap reduction functions exhibit a remarkably simple structure, enabling novel and direct tests of scalar polarizations with these experiments. In what follows we focus on tensor and breathing scalar polarizations, since the case of vector modes is straightforward.

A large body of work has already investigated the response of PTAs and astrometry to GWs, see, e.g., [8] for a review. Our results extend these efforts by introducing three-point correlation functions into PTA and astrometry analyses, with the aim to extract effects of GW scalar polarization.

1. Pulsar timing arrays

For PTAs, we compute correlators of the GW-induced redshift in the pulse arrival rate, given by (see, e.g., [2] for a textbook discussion)

$$z(t) = \frac{n^i n^j}{2(1+\mathbf{n}_a\cdot\mathbf{n})}\left[h_{ij}(t,\mathbf{x}=0) - h_{ij}(t-\tau_a,\mathbf{x}_a)\right], \tag{2.24}$$

where τ_a is the light travel time between Earth and pulsar a, $\mathbf{n}_a$ is the unit vector pointing toward pulsar a, and $\mathbf{n}$ is the unit vector indicating the GW propagation direction.

We begin by recalling (without derivation) the known results for two-point correlators, following the approach of [2]. Denoting again by $I_T(f)$ and $I_b(f)$ the intensities associated with tensor and breathing scalar polarizations, the ensemble average of two PTA measurements is

$$\langle z_a(t) z_b(t)\rangle = \frac{1}{2}\int_{-\infty}^{\infty} df\left[I_T(f)\kappa_{ab}^{\rm tens}(\theta_{ab}) + I_b(f)\kappa_{ab}^{\rm scal}(\theta_{ab})\right], \tag{2.25}$$

where the overlap reduction functions $\kappa^{\rm tens}$ and $\kappa^{\rm scal}$ are obtained by integrating over all GW directions. Neglecting pulsar terms, the tensor overlap function reduces to the Hellings-Downs curve [56],

$$\kappa_{ab}^{\rm tens}(\theta_{ab}) = x_{ab}\log x_{ab} - \frac{1}{6}x_{ab} + \frac{1}{3}, \tag{2.26}$$

with

$$x_{ab} = \frac{1}{2}(1-\cos\theta_{ab}),$$

where $\theta_{ab} = \arccos(\hat{n}_a\cdot\hat{n}_b)$ is the angular separation between pulsars a and b. The scalar overlap function instead reads (see, e.g., [8])

$$\kappa_{ab}^{\rm scal}(\theta_{ab}) = \frac{1}{6}(2-x_{ab}). \tag{2.27}$$

We now extend this construction to higher-order correlators. The three-point correlator of PTA measurements is

$$\langle z_a(t) z_b(t) z_c(t)\rangle = \frac{1}{2}\int_{-\infty}^{\infty} df\left[B_T(f)\kappa_{abc}^{\rm tens}(\mathbf{n}_a,\mathbf{n}_b,\mathbf{n}_c) + B_b(f)\kappa_{abc}^{\rm scal}(\mathbf{n}_a,\mathbf{n}_b,\mathbf{n}_c)\right], \tag{2.28}$$

where B_T and B_b are the tensor and scalar bispectra [see Eq. (2.8)], and $\mathbf{n}_{a,b,c}$ denote the pulsar directions. The overlap functions are

$$\kappa_{abc}^{\rm tens}(\mathbf{n}_a,\mathbf{n}_b,\mathbf{n}_c) = \frac{1}{2\pi}\int_0^{2\pi} d\psi \int d^2\hat{n} \sum_{\lambda=+,\times} F_a^\lambda(\mathbf{n}_a) F_b^\lambda(\mathbf{n}_b) F_c^\lambda(\mathbf{n}_c), \tag{2.29}$$

$$\kappa_{abc}^{\rm scal}(\mathbf{n}_a,\mathbf{n}_b,\mathbf{n}_c) = \frac{1}{2\pi}\int_0^{2\pi} d\psi \int d^2\hat{n} F^{\rm b}(\mathbf{n}_a) F^{\rm b}(\mathbf{n}_b) F^{\rm b}(\mathbf{n}_c), \tag{2.30}$$

with antenna response functions

$$F^\sigma(\mathbf{n}_k) = \frac{n_k^i n_k^j}{2(1+\mathbf{n}\cdot\mathbf{n}_k)} e_{ij}^\sigma, \tag{2.31}$$

for $\sigma = \{+,\times,{\rm b}\}$, where k labels the pulsar.

Exploiting rotational freedom, we fix Earth at the origin, place pulsar a on the z-axis, pulsar b in the xz plane, and pulsar c at generic angles (χ_1,χ_2), see Fig. 2,

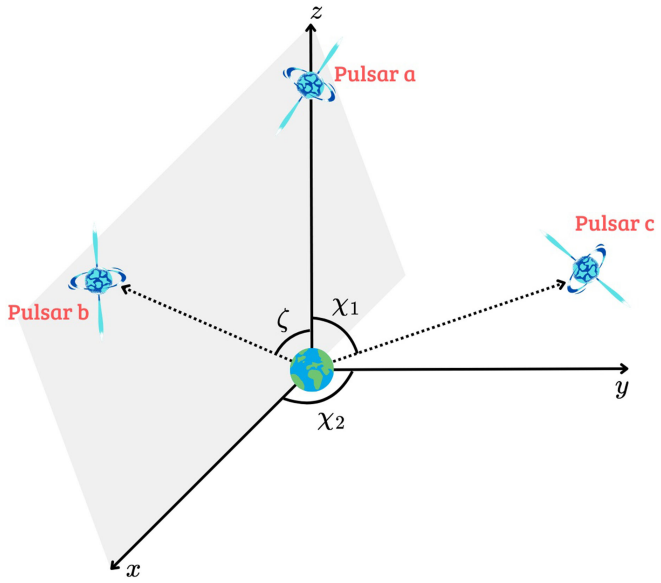

FIG. 2. Geometry used to compute three-point overlap functions from pulsars a, b, and c. Earth is at the origin, pulsar a is placed on the z-axis, pulsar b lies in the xz plane, and pulsar c is at a generic position.

$$\mathbf{n}_a = (0,0,1), \qquad \mathbf{n}_b = (\sin\zeta, 0, \cos\zeta),$$
$$\mathbf{n}_c = (\sin\chi_1\cos\chi_2, \sin\chi_1\sin\chi_2, \cos\chi_1). \tag{2.32}$$

With this configuration, $\kappa^{\rm tens}_{abc} = 0$ after integration over the polarization angle ψ, consistent with the arguments of Sec. II A. The scalar overlap function reduces to

$$\kappa^{\rm scal}_{abc}(\mathbf{n}_a, \mathbf{n}_b, \mathbf{n}_c) = \frac{1}{12}(3 + \mathbf{n}_a\cdot\mathbf{n}_b + \mathbf{n}_a\cdot\mathbf{n}_c + \mathbf{n}_b\cdot\mathbf{n}_c). \tag{2.33}$$

This remarkably simple expression generalizes in an intuitive way the two-point result of Eq. (2.16). In fact, it maintains the monopolar structure of a response function (in contrast with the typical quadrupolar ones found in Einstein gravity).

2. Astrometry

Astrometry provides a complementary probe of GW effects (see, e.g., [57–81]). Following the notation of [61], the GW induces an apparent angular deflection

$$\delta n_i(\mathbf{n}_a, t) = \mathcal{R}_{ijk}(\mathbf{n}_a, \mathbf{n}) h_{jk}(t, 0), \tag{2.34}$$

in the direction of a star $\mathbf{n}_a$, where $\mathbf{n}$ is the GW propagation direction. The response tensor is

$$\mathcal{R}_{ijk}(\mathbf{n}_a, \mathbf{n}) = \frac{n_{aj}}{2}\left[\frac{(n_{ai} + n_i)n_{ak}}{1 + \mathbf{n}_a\cdot\mathbf{n}} - \delta_{ik}\right]. \tag{2.35}$$

The equal-time three-point correlation of stellar deflections is then

$$\langle \delta n_i(\mathbf{n}_a)\delta n_j(\mathbf{n}_b)\delta n_k(\mathbf{n}_c)\rangle = \mathcal{A} H_{ijk}(\mathbf{n}_a, \mathbf{n}_b, \mathbf{n}_c), \tag{2.36}$$

where $\mathcal{A}$ encodes integrals over the GW background, and

$$H_{ijk}(\mathbf{n}_a, \mathbf{n}_b, \mathbf{n}_c) = \int d^2\hat{n}\, \mathcal{K}_i(\mathbf{n}_a)\mathcal{K}_j(\mathbf{n}_b)\mathcal{K}_k(\mathbf{n}_c), \tag{2.37}$$

with

$$\mathcal{K}_i(\mathbf{n}_a) = \mathcal{R}_{ijk}(\mathbf{n}_a) e^{\lambda}_{jk}, \tag{2.38}$$

with λ the polarization index. We find that performing the angular integral yields $H_{ijk} = 0$ for all polarizations, scalars included. Hence, astrometry alone possesses no nontrivial three-point overlap function and can instead serve as a null channel for noise characterization.

3. Cross-correlations between PTA and astrometry

The situation changes when pulsars and stars are cross-correlated. In this case, three-point overlap functions for scalar polarizations are generically nonvanishing and might be exploited to detect GW signals. In fact, cross-correlations are especially useful to calibrate measurements and reduce systematics.

For the correlation of two stars and one pulsar, with $\mathbf{n}_{s_i}$ the direction of the ith star and $\mathbf{n}_p$ the pulsar direction, we obtain

$$\langle \delta n(\mathbf{n}_{s_1}, t)\delta n(\mathbf{n}_{s_2}, t')z(\mathbf{n}_p, f)\rangle = \mathcal{A}(f) H_0(\mathbf{n}_{s_1}, \mathbf{n}_{s_2}, \mathbf{n}_p), \tag{2.39}$$

with

$$\mathbf{H}_0(\mathbf{n}_{s_1}, \mathbf{n}_{s_2}, \mathbf{n}_p) = \int d^2\Omega \mathcal{K}_i(\mathbf{n}_{s_1})\mathcal{K}_j(\mathbf{n}_{s_2}) F^{\rm b}(\mathbf{n}_p), \tag{2.40}$$

where $\mathcal{K}_i$ is given in Eq. (2.38) with $\lambda = b$, and $F^{\rm b}$ is the PTA breathing-mode response defined in Eq. (2.31). The angular integral evaluates to the following matrix components

$$H_{0ij}(\mathbf{n}_{s_1}, \mathbf{n}_{s_2}) = \frac{\pi}{6}[\delta_{ij} - n^{s_1}_i n^{s_1}_j - n^{s_2}_i n^{s_2}_j + (\mathbf{n}^{s_1}\cdot\mathbf{n}^{s_2}) n^{s_1}_i n^{s_2}_j], \tag{2.41}$$

which coincides with the two-point astrometry correlation of [27] and is independent of the PTA position. Curiously, the combination of scalar spin-0 polarization tensors in the previous three-point expression manages to mimic the effect of tensor spin-2 in the two-point reduction function. It would be interesting to find a physical interpretation for this fact. Figure 3 illustrates $\mathrm{Tr}[\mathbf{H}_0\mathbf{H}_0]$.

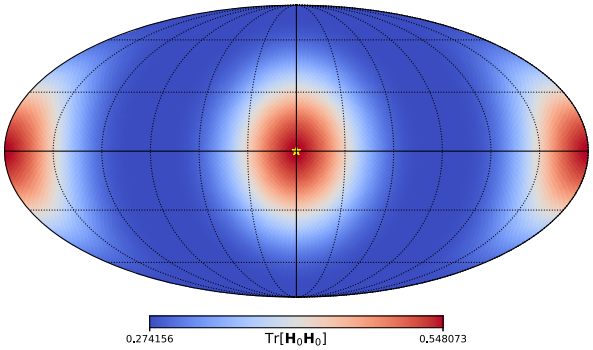

FIG. 3. Mollweide projection of $\mathrm{Tr}[\mathbf{H}_0\mathbf{H}_0]$ which correlates two stars with a pulsar position, see Eq. (2.41). The result depends only on the star positions. For illustrative reasons, we fix one star at the center of the plot, and we allow the direction of the second to vary across the sky.

Similarly, the correlation of two pulsars and one star is nonvanishing only for scalar polarizations. Restricting again to the breathing scalar mode, we find

$$\langle z(\mathbf{n}_{p_1}) z(\mathbf{n}_{p_2}) \delta n(\mathbf{n}_s)\rangle = \mathcal{A}(f)\mathbf{K}_0(\mathbf{n}_{p_1},\mathbf{n}_{p_2},\mathbf{n}_s), \tag{2.42}$$

with the vector $\mathbf{K}_0$ given by

$$\mathbf{K}_0(\mathbf{n}_s,\mathbf{n}_{p_1},\mathbf{n}_{p_2}) = \int d^2\hat{n}\mathcal{K}_i(\mathbf{n}_s)F^{\mathrm{b}}(\mathbf{n}_{p_1})F^{\mathrm{b}}(\mathbf{n}_{p_2}), \tag{2.43}$$

which evaluates to

$$\mathbf{K}_0(\mathbf{n}_s,\mathbf{n}_{p_1},\mathbf{n}_{p_2}) = \frac{\pi}{6}[(\mathbf{n}_{p_1}\times\mathbf{n}_s)\times\mathbf{n}_s + (\mathbf{n}_{p_2}\times\mathbf{n}_s)\times\mathbf{n}_s]. \tag{2.44}$$

Hence, again, a mathematically simple expression—which this time depends on the position of all three objects involved. The associated structure $\mathbf{K}_0\cdot\mathbf{K}_0^T$ is shown in Fig. 4.

4. Summary

In summary, we have obtained the three-point overlap reduction functions for PTA and astrometry. Overlap functions vanish for tensor and vector polarizations but are generically nonvanishing for scalar polarizations. We discussed their geometrical interpretation, if any, in terms of properties of scalar-polarization tensors. We point out that mixed correlators (tensor-tensor-scalar or vector-vector-scalar) can also be nonzero, but a scalar mode must always be present. Thus, any nonvanishing detection of a three-point correlation function would provide a clear and distinctive signature of scalar GW polarizations.

III. DETECTING A GRAVITATIONAL WAVE THREE-POINT FUNCTION

In the previous section we discussed the response of gravitational wave detectors to the GW three-point function—mostly focusing on pulsar timing arrays and astrometry—and pointed out their potential use as a smoking gun for scalar polarizations. We now examine a convenient estimator for this observable. We correspondingly design a simple likelihood function, and we develop preliminary Fisher forecasts in an idealized situation, so to explore the detectability of GW three-point function with pulsar timing array measurements.

A. Building an optimal estimator

We construct an optimal estimator for the GW three-point function, following the approach of [38], but adapting it to the case of scalar modes. For building such estimator, in this section we keep our discussion general, and we do not need to specify the GW detector we focus on. Let

$$\Sigma(t) = s(t) + n(t) \tag{3.1}$$

denote the time-domain output of a single GW detector, where $s(t)$ is the gravitational wave signal and $n(t)$ represents the instrumental noise. We consider the cross-correlation of *three* such measurements $\Sigma(t)$, assuming that the noise $n(t)$ is stationary, Gaussian, and uncorrelated

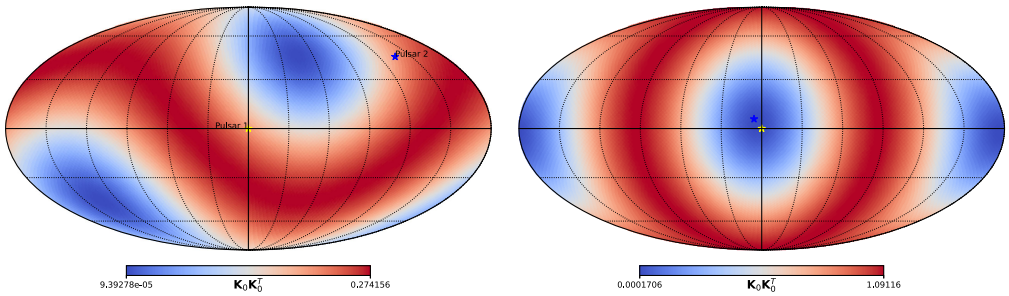

FIG. 4. Mollweide projection of $\mathbf{K}_0\cdot\mathbf{K}_0^T$ from Eq. (2.44), for different pulsar-star configurations. In both panels, the first pulsar is fixed at the center. Left: the case where the second pulsar is far from the first. Right: the case where the two pulsars are close to each other. Correspondingly, in both plots we vary the position of the star.

between different detectors.[6] We focus on the noise-dominated regime, in which the variance is set by the noise, while the expectation value of the statistic is determined entirely by the signal $s(t)$. Signals from different detectors may exhibit non-Gaussian correlations with nonvanishing three-point functions $\langle s^3\rangle$, assumed to be stationary as in the hypothesis outlined in Sec. II.

A combination of three copies of $\Sigma(t)$ provides the estimator we are interested to study, which we use to test the presence of scalar polarizations in GW. We build the quantity

$$S_{abc} = \int_{-T/2}^{T/2} dt_1 \int_{-T/2}^{T/2} dt_2 \times \int_{-T/2}^{T/2} dt_3 \Sigma_a(t_1)\Sigma_b(t_2)\Sigma_c(t_3) Q(t_2 - t_1, t_3 - t_1), \tag{3.2}$$

where T is the time duration of our measurement, and Q is a filter function—to be determined—depending only on the time differences given we work on the hypothesis of stationarity. It vanishes for large separations $|t_i - t_j|$. The goal is to choose the filter function Q to maximize the response to the signal. For the moment, we focus on a single triplet of measurements (abc) with three different GW detectors.

We Fourier transform the time series as

$$\Sigma(t) = \int df e^{2\pi i f t} \tilde{\Sigma}(f), \tag{3.3}$$

which yields

$$S_{abc} = \int df_1 df_2 df_3 \delta_T(f_1 + f_2 + f_3) \times \tilde{\Sigma}_a(f_1)\tilde{\Sigma}_b(f_2)\tilde{\Sigma}_c(f_3)\tilde{Q}^*(f_2, f_3), \tag{3.4}$$

where we have introduced the finite-time δ function (and T the measurement duration)

$$\delta_T(f) \equiv \int_{-T/2}^{T/2} dt e^{2\pi i f t}, \qquad \delta_T(0) = T. \tag{3.5}$$

In the noise-dominated regime, the mean and variance of S_{abc} are

$$\mu = \langle S_{abc}\rangle, \tag{3.6}$$

$$\sigma^2 = \langle S_{abc}^2\rangle - \mu^2. \tag{3.7}$$

[6]A Gaussian noise hypothesis allows us—by measuring signal three-point functions—to avoid systematic uncertainties on pulsar timing and Solar System ephemeris which can affect measurements of two-point correlation functions. We point out though that recent interesting analyses are taking into account more general possibilities for noise statistics—see, e.g., [82–86].

Since the noise is Gaussian, μ is determined solely by the signal, while σ^2 is determined by the noise [which we assume much larger in amplitude than the signal—hence we can neglect the contribution proportional to μ^2 in Eq. (3.6)]. The signal-to-noise ratio (SNR) reads

$$\mathrm{SNR} = \frac{\mu}{\sigma} \tag{3.8}$$

and constitutes the quantity to maximize by appropriately choosing the filter function.

A direct calculation gives

$$\mu = T\kappa_{abc} \int df_1 df_2 B_b(f_1, f_2, f_3)\tilde{Q}^*(f_1, f_2), \tag{3.9}$$

where κ_{abc} is the three-detector overlap reduction function and $B_b(f_1, f_2, f_3)$ is the breathing-mode bispectrum defined in Eq. (2.8), satisfying[7] the condition $f_1 + f_2 + f_3 = 0$. Indicating with $\sigma_a^2(f_1)$ the noise spectrum, the noise two-point function is defined as

$$\langle n_a(f_1) n_b(f_2)\rangle = \delta(f_1 + f_2)\delta_{ab}\sigma_a^2(f_1), \tag{3.10}$$

leading to the total variance (recall that we work under the hypothesis that the noise has Gaussian distribution)

$$\sigma^2 = T \int df_1 df_2 N_{abc}(f_1, f_2)|Q(f_1, f_2)|^2, \tag{3.11}$$

where

$$N_{abc}(f_1, f_2) \equiv \sigma_a^2(f_1)\sigma_b^2(f_2)\sigma_c^2(f_1 + f_2) + \text{perms}. \tag{3.12}$$

Thus, the SNR becomes

$$\mathrm{SNR} = \sqrt{T}\frac{\kappa_{abc}\int df_1 df_2 B_b(f_1, f_2)\tilde{Q}^*(f_1, f_2)}{[\int df_1 df_2 N_{abc}(f_1, f_2)|Q(f_1, f_2)|^2]^{1/2}}. \tag{3.13}$$

Adopting the Wiener filtering technique (see, e.g., [54] for a clear discussion in a similar context), we introduce the positive-definite inner product

$$(C, D) \equiv \int df_1 df_2 C(f_1, f_2) D^*(f_1, f_2) N_{abc}(f_1, f_2), \tag{3.14}$$

so that

$$\mathrm{SNR} = \sqrt{T}\frac{(\kappa_{abc}B_b/N_{abc}, Q)}{[(Q, Q)]^{1/2}}. \tag{3.15}$$

[7]Since $f_3 = -f_1 - f_2$, in what follows we understand the dependence of f_3 on B_b.

The optimal filter we are searching for is then

$$Q(f_1, f_2) = \frac{\kappa_{abc} B_b(f_1, f_2)}{N_{abc}(f_1, f_2)}, \tag{3.16}$$

which yields the maximum achievable SNR in our context,

$$\mathrm{SNR}_{\max} = \sqrt{T}\left[\int df_1 df_2 \frac{(\kappa_{abc} B_b(f_1, f_2))^2}{N_{abc}(f_1, f_2)}\right]^{1/2}. \tag{3.17}$$

A further simplification occurs for frequency-independent noise, $\langle n_a(f_1) n_b(f_2)\rangle = \delta(f_1 + f_2)\delta_{ab}\sigma_a^2$, in which case

$$N_{abc}(f_1, f_2) = 3\sigma_a^2\sigma_b^2\sigma_c^2 \tag{3.18}$$

and

$$\mathrm{SNR}_{\max} = \sqrt{\frac{T}{3}}\left[\int df_1 df_2 \frac{(\kappa_{abc} B_b(f_1, f_2))^2}{\sigma_a^2\sigma_b^2\sigma_c^2}\right]^{1/2} \tag{3.19}$$

for measurements from a single triplet of detectors. If multiple GW detector triplets are, in principle, available—as in the case of PTAs—we can increase the total SNR by summing over all possible combinations.

In summary, we have constructed an optimal estimator for detecting the scalar bispectrum B_b, which serves as a direct diagnostic of scalar polarizations in the SGWB signal. The procedure consists of forming a suitable combination of three measurements $\Sigma(t)$ and integrating over time, see Eq. (3.2). After Fourier transforming and applying the optimal filter defined in Eq. (3.16), we obtain the best possible measurement of B_b. On this basis, we next develop a simple forecast for the detectability of scalar polarizations with idealized future PTA measurements, employing the Fisher formalism.

B. Fisher forecasts for detecting scalar polarizations with PTA

Based on the results we derived above and under a set of simplifying assumptions we are going to describe, we construct a likelihood for our estimator of scalar polarizations in GW experiments. Such likelihood might serve as the basis for deriving idealized Fisher forecasts for the detectability of scalar modes with PTA by taking signal three-point functions.

We focus on measuring the scalar bispectrum B_b, see Eq. (2.8), as a diagnostic of the presence of scalar polarizations. For simplicity, in this section we assume a "power-law" behavior for this quantity,[8] with an ansatz

$$B_b(f_1, f_2) = \frac{P_0^3}{f_1^{3-n_1} f_2^{3-n_2}} \tag{3.20}$$

parametrized by two spectral indexes $n_{1,2}$ in Eq. (3.22). We indicate the bispectrum amplitude as cube P_0^3 to indicate it originates from a three-point function—an explicit example is developed in Sec. IV.

We would like to quantify the bispectrum amplitude P_0 which can, in principle, be measured with PTA data, under the simple ansatz above. We assume that the likelihood for B_b follows a Gaussian distribution, with variance determined by the experimental noise properties described earlier. Hence our approach extends that of [87–91], which considered Gaussian likelihoods for the intensity and polarization of the SGWB in the context of PTAs. We write the logarithm of the likelihood $\mathcal{L}$ as

$$-2\ln\mathcal{L} = \mathrm{const} + \sum_{f_1,f_2}\sum_{AB}(\mathcal{R}_A - \kappa_A \cdot B_s) \times C_{AB}^{-1}(\mathcal{R}_B - \kappa_B \cdot B_s), \tag{3.21}$$

where $\mathcal{R}_A$ is the Fourier transform of time-integrated three-point functions of GW measurements, and the sums are over pulsar triplets, denoted by $A = (abc)$. The dot denotes the integrated quantity

$$\kappa_A \cdot B_s = P_0^3 \kappa_A \int_{f_1-\Delta f/2}^{f_1+\Delta f/2}\int_{f_2-\Delta f/2}^{f_2+\Delta f/2} \frac{d\tilde{f}_1 d\tilde{f}_2}{\tilde{f}_1^{3-n_1}\tilde{f}_2^{3-n_2}}, \tag{3.22}$$

generalizing [90,91] to the case of the bispectrum. Each integration runs over a small frequency interval Δf, and the sum in Eq. (3.21) covers all such intervals. The quantity κ_A denotes the PTA response to scalar polarizations in three-point measurements, as in Eq. (2.33).

The inverse covariance matrix is deduced from the results of Sec. III A. Assuming, for simplicity, that all pulsars are monitored over the same observation time T, we have

$$C_{AB}^{-1} = \frac{2T\Delta f^2}{3\mathbf{R}_A^N\mathbf{R}_B^N}\delta_{AB}, \tag{3.23}$$

where A, B denote pulsar triplets. This quantity also depends on the frequency interval Δf used to bin the frequency bands, over which we sum. The factors $\mathbf{R}_A^N$ in the previous equation encode the intrinsic pulsar noise and in the weak-signal limit we obtain

$$\mathbf{R}_A^N \simeq (\sigma_a^2\sigma_b^2\sigma_c^2)^{1/2}, \tag{3.24}$$

with σ_a the band-integrated noise variance of pulsar a.

Starting from the likelihood (3.21), we compute the Fisher matrix associated with the parameters of interest. In this initial study, we focus on the single parameter, the amplitude P_0 of the bispectrum with structure as in Eq. (3.22). We keep the spectral indexes $n_{1,2}$ fixed, and we estimate the sensitivity of measurements to P_0. The (single) Fisher matrix

[8] In Sec. IV we discuss a more realistic cosmological setup leading to a richer structure for the scalar-polarization bispectrum. Our analysis can be straightforwardly extended to that case, as well as to other theoretically motivated setups.

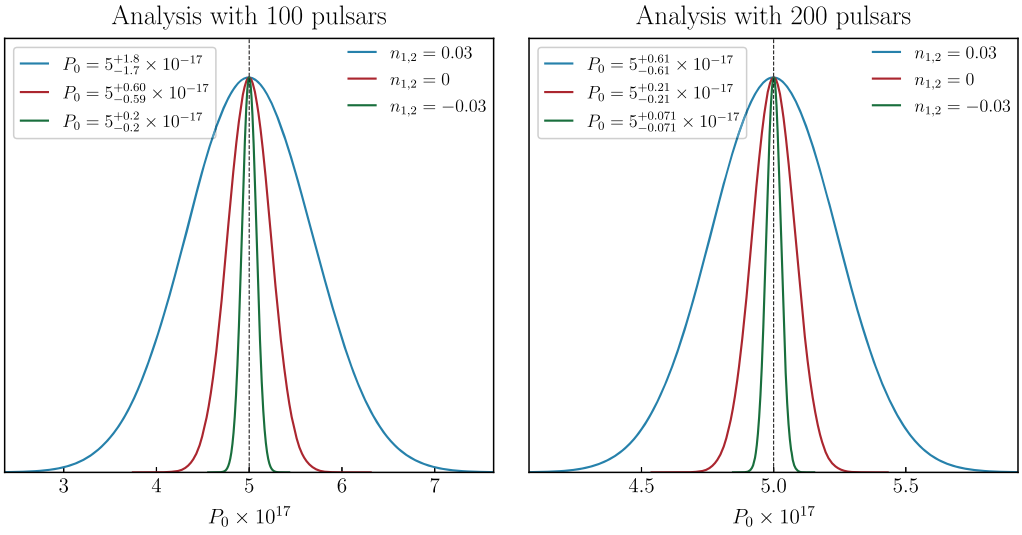

FIG. 5. Constraints on the parameter P_0 of Eq. (3.22) at 3-σ confidence level from the Fisher forecast described in Sec. III B. In the two plots we represent results for two pulsar populations and different choices of spectral indices. We take $n_1 = n_2$ in the cases shown. The confidence intervals are displayed in the left box of each panel. In all cases, the fiducial value is fixed to $P_0 = 5 \times 10^{-17}$.

component for each frequency bin Δf is summed over all bins and all pulsar triplets,

$$\mathcal{F}_{P_0P_0} = \left\langle -\frac{\partial^2 \ln \mathcal{L}}{\partial P_0^2} \right\rangle = \sum_{f_1,f_2} \sum_{AB} \frac{2T\Delta f^2}{\mathbf{R}_A^N \mathbf{R}_B^N} \left(\frac{6P_0^4 \kappa_A \kappa_B \delta_{AB}}{f_1^{6-2n_1} f_2^{6-2n_2}} \right). \tag{3.25}$$

For the forecast, we adopt a frequency binning of $\Delta f = 1/T$, with a common observation time of $T = 15$ yr. As representative experimental setup, we take the noise amplitude associated with pulsar J1012-4235 from the NG15 results [92] as the common noise model for all pulsars. For simplicity we assume pulsars are randomly distributed on the sky, and we consider two ensembles of 100 and 200 pulsars as representative of forthcoming PTA experiments. We find that the results are very sensitive to the spectral indices $n_{1,2}$, indicating that the frequency dependence of the bispectrum plays an important role in determining its observability. Hence, the results of measurements will depend on the theoretical models one considers. The forecasts are summarized in Fig. 5 obtained using the GetDist package [93], where we learn that values of P_0 of order 5×10^{-17} are, in principle, detectable, with variations in the error bar size of order unity depending on the number of pulsars and on the spectral indices n_1, n_2 in Eq. (3.22).

Although this simple Fisher analysis can be improved in several directions, it provides a concrete illustration that, in principle, measuring the GW three-point function can serve as a useful diagnostic of scalar polarizations, provided the bispectrum amplitude is sufficiently large to be detectable.

IV. A COSMOLOGICAL SOURCE FOR THREE-POINT FUNCTIONS

After outlining in general terms how measurements of the GW three-point function can reveal the presence of scalar polarizations, in this section we develop an explicit cosmological example that can generate an enhanced three-point function for scalar GW modes. Such setup might be used as benchmark cosmological scenario to search for additional polarizations in the SGWB implementing our method. Cosmological sources of the SGWB (see [9] for a comprehensive review) may account for at least part of the PTA-detected SGWB signal—see, e.g., the early studies [94,95]. If this were the case, it may be, of course, unfeasible to apply methods that rely on assumptions about black hole merger waveforms (see, e.g., the recent [96] and references therein) in order to extract information on additional polarizations. The possibility of cosmological sources contributing to the SGWB then further motivates the new approach introduced in this work.

A. Second-order perturbations and gravitational waves

We expect that any nonlinear source of a stochastic gravitational wave background produces non-Gaussianities in the signal. If detectable, such non-Gaussian features can yield valuable insights into the physical origin of the SGWB, as well as important information about the underlying theory of gravitational interactions. Indeed, a variety of theoretical studies have quantified GW non-Gaussianity from both cosmological and astrophysical sources and explored its possible observational signatures—see Sec. II B.

In this work we investigate, for the first time, tensor non-Gaussianities in a cosmological setup based on GW induced at second-order fluctuations, a framework which leads to a particularly transparent and instructive calculation. Our aim here is twofold:

(1) Apply the theoretical approach of second-order induced GWs to the case of extra GW polarizations, with the aim of testing the existence of additional polarizations in GW measurements through the methods discussed in the previous sections.[9]
(2) Clarify the importance of stationary three-point functions for obtaining a measurable signal, explicitly addressing in this context arguments first developed in [42].

If gravitational waves carry extra polarizations—beyond the spin-2 modes of general relativity—they are sourced at second order by fluctuations of a Gaussian field in the early Universe, in complete analogy with the standard generation of spin-2 polarizations. Instead of the more commonly considered scalar perturbations, we focus on a spectator vector source, which will turn out to be easier to handle for our purposes. Schematically, the GW tensor perturbation h_{ij} is sourced by an operator quadratic in a vector field v_i,

$$h_{ij} \sim v_i v_j, \tag{4.1}$$

so that the GW two- and three-point functions are proportional to the vector four- and six-point functions, respectively. Applying Wick's theorem, a $2n$-point function of a Gaussian vector field decomposes into products of n two-point functions. In addition to the case $n = 2$ (yielding the GW power spectrum), for our purposes we also examine the bispectrum case with $n = 3$.

1. Primordial magnetic fields as GW source

We illustrate this mechanism in a context motivated by primordial magnetogenesis. This framework postulates that cosmological magnetic fields—capable of explaining the observed large-scale magnetic fields in the Universe—were generated during cosmic inflation. See, e.g., [98] for a review. We assume that some early-Universe process produces a large-scale magnetic field $\mathbf{B}$, which in turn sources the physical GW polarizations at second order in perturbations. To compute the resulting GW signal, we adapt the methods already developed for scalar-induced GW scenarios, where enhanced curvature perturbations source GWs after inflation. This line of research has a long history; see [99] for a review and [100,101] for recent techniques for reconstructing the signal. Here we apply the formalism to the nonadiabatic case of magnetic-field sources, as studied in several earlier works [102–110], and initiate the calculation of the GW bispectrum for the scalar (breathing) polarization in this context. We expand the breathing-mode contribution to the GW in Fourier space as[10]

$$h_{ij}(\tau, \mathbf{x}) = \int \frac{d^3\mathbf{k}}{(2\pi)^{3/2}} e^{i\mathbf{k}\cdot\mathbf{x}} \mathbf{e}_{ij}^{(b)}(\mathbf{k}) h_{\mathbf{k}}(\tau), \tag{4.2}$$

where we retain only the scalar breathing mode, which is the focus of our analysis since only the presence of scalar polarization can lead to nonvanishing detector-response functions in the case of three-point functions (recall Sec. II).

Since the magnetic field is governed by the Maxwell action in curved spacetime—quadratic in the vector fields—we assume that it obeys Gaussian statistics, with a two-point function satisfying the relation [104]

$$\langle B_i(\mathbf{k}) B_j(\mathbf{q}) \rangle'_{\mathbf{k}+\mathbf{q}=\mathbf{0}} = B_0 \pi_{ij}(\mathbf{k}) f(k), \tag{4.3}$$

where the prime indicates that the momentum-conserving δ function has been omitted. We place as overall factor a constant B_0—which characterizes the magnetic spectrum amplitude at large scales in appropriate units—and we denote as π_{ij} the symmetric tensor

$$\pi_{ij}(\mathbf{k}) = \delta_{ij} - \frac{k_i k_j}{k^2}, \tag{4.4}$$

with $k = \sqrt{\mathbf{k}\cdot\mathbf{k}}$. We indicate with $f(k)$ a (model-dependent) dimensionless function controlling the scale dependence of the magnetic spectrum, normalizing it by imposing it has unit value at large, cosmic microwave background scales: $f(k_{\rm CMB}) = 1$. While often a simple power-law scaling is assumed for $f(k)$, one can also consider richer scenarios, as, e.g., [111].

The magnetic field acts as a source term for the scalar polarization in the GW evolution equation in Fourier space [recall the Fourier mode definition of Eq. (4.2)],

$$h''_{\mathbf{k}} + 2\mathcal{H} h'_{\mathbf{k}} + k^2 h_{\mathbf{k}} = \frac{S_{\mathbf{k}}}{a^2(\tau)}, \tag{4.5}$$

where $S_{\mathbf{k}} = e_{ij}^{(b)} \tau_{ij}^{(B)}$, and the magnetic-field energy-momentum tensor is (see, e.g., [104])

$$\tau_{ij}^{(B)}(\mathbf{k}) = \frac{1}{4\pi} \int \frac{d^3\mathbf{p}}{(2\pi)^3} \left[B_i(\mathbf{p}) B_j(\mathbf{k}-\mathbf{p}) - \frac{\delta_{ij}}{2} B_m(\mathbf{p}) B_m(\mathbf{k}-\mathbf{p}) \right]. \tag{4.6}$$

[9] See also the study [97] which explores scalar-induced gravitational waves in alternative theories of gravity.

[10] In this section, in order to align with the literature on field-theoretic treatments of second-order GW sources, we perform a Fourier transform over the three spatial dimensions, rather than the four-dimensional transform employed in Sec. II.

Notice that the scalar polarization tensor $\mathbf{e}_{ij}^{(b)}(\hat{k}) = \pi_{ij}(\hat{k})$ projects the magnetic-field energy moment tensor along the components of the breathing scalar mode. The source term becomes

$$S_{\mathbf{k}}(\tau) = -\frac{1}{4\pi k^2}\int \frac{d^3\mathbf{p}}{(2\pi)^3}[\mathbf{k}\cdot\mathbf{B}(\mathbf{p})][\mathbf{k}\cdot\mathbf{B}(\mathbf{k}-\mathbf{p})]. \quad (4.7)$$

Equation (4.5) can be solved formally as

$$h_{\mathbf{k}}(\tau) = \frac{1}{a(\tau)}\int_{\tau_R}^{\tau} d\tau' \frac{g_k(\tau,\tau')}{a(\tau')} S_{\mathbf{k}}(\tau'), \quad (4.8)$$

where g_k is the Green's function for the system under consideration. In what follows, we focus on radiation domination, and τ_R denotes the time of instantaneous reheating at the end of inflation. Equation (4.8) makes precise the schematic relation (4.1), showing that the GW signal is indeed sourced by the quadratic combination of vector modes. During radiation domination,

$$g_k(\tau,\tau') = \frac{1}{k}[\sin(k\tau)\cos(k\tau') - \sin(k\tau')\cos(k\tau)]. \quad (4.9)$$

On this basis, we now proceed to compute explicitly the two- and three-point functions of the GW solution in Eq. (4.8). We expect that these correlators depend on the square and the cube of the magnetic vector source, hence—according to Eq. (4.3)—they are proportional to B_0^2 and B_0^3, respectively.

B. The gravitational wave two-point function

The GW two-point function is a key observable, as it is directly related to the GW energy density. Several works [102–110] have investigated how primordial magnetic fields can act as a source for this quantity. As a warm-up, we extend here the discussion of [111] to the computation of two-point correlators involving scalar polarizations, as induced by primordial magnetic fields. This case provides a useful starting point, since it will be straightforwardly generalized to the three-point function in Sec. IV C.

We write the GW scalar-polarization power spectrum as

$$\begin{aligned} P_h(k) &\equiv \langle h_{\mathbf{k}}(\tau)h_{\mathbf{q}}(\tau)\rangle'_{\mathbf{k}=-\mathbf{q}} \\ &\equiv \frac{1}{a^2(\tau)}\int d\tau_1 d\tau_2 \frac{g_k(\tau,\tau_1)}{a(\tau_1)}\frac{g_q(\tau,\tau_2)}{a(\tau_2)}\langle S_{\mathbf{k}}S_{\mathbf{q}}\rangle'_{\mathbf{k}=-\mathbf{q}} \\ &= \frac{1}{a^2(\tau)}\mathcal{I}_{(2)}(\tau)\langle S_{\mathbf{k}}S_{\mathbf{q}}\rangle'_{\mathbf{k}=-\mathbf{q}}, \end{aligned} \quad (4.10)$$

with

$$\mathcal{I}_{(2)}(k,\tau) = \left(\int_{\tau_R}^{\tau} d\tau_1 \frac{g_k(\tau,\tau_1)}{a(\tau_1)}\right)^2. \quad (4.11)$$

We evaluate the result at late times, $\tau/|\tau_R| \gg 1$, during radiation domination. These expressions are structurally similar to the formulas obtained for spin-2 polarizations, differing only by overall coefficients arising from distinct polarization tensors.

Equation (4.10) shows that the time and momentum integrals factorize: all the time dependence is contained in $\mathcal{I}_{(2)}$, while the momentum dependence resides in the source two-point function $\langle S_{\mathbf{k}}S_{\mathbf{q}}\rangle'_{\mathbf{k}+\mathbf{q}=0}$. This separation is especially convenient, since the two quantities can be computed independently—a property which will be especially useful in Sec. IV C when discussing the detectability of the signal three-point correlators.

1. The time integral

We begin with the time integral in Eq. (4.11), evaluated in the limit of large conformal time τ, well within the radiation-dominated era. This expression produces contributions involving $\sin(k\tau)$, $\cos(k\tau)$, and their squares. Terms linear in these oscillatory functions vanish upon averaging over rapid oscillations, whereas quadratic terms average to $1/2$. The result is

$$\mathcal{I}_{(2)}(k,\tau) = \frac{1}{2k^2a^4H^2}\left[\mathrm{Ci}(-k\tau_R)^2 + \left(\frac{\pi}{2} - \mathrm{Si}(-k\tau_R)\right)^2\right], \quad (4.12)$$

where $\mathrm{Ci}(x)$ and $\mathrm{Si}(x)$ denote the cosine and sine integral functions, respectively. This expression exhibits a logarithmic divergence for small $|k\tau_R|$, since $\mathrm{Ci}(x) \sim \ln(x)$ as $x \to 0$.

2. Contributions from the source

We now turn to the source two-point function, which takes the form of a convolution integral,

$$\begin{aligned} \langle \bar{S}_{\mathbf{k}}\bar{S}_{\mathbf{q}}\rangle'_{\mathbf{k}+\mathbf{q}=\mathbf{0}} &= \frac{k_a k_b k_c k_d}{(4\pi)^2 k^4}\int \frac{d^3\mathbf{p_1}}{(2\pi)^3} \\ &\quad\times \int \frac{d^3\mathbf{p_2}}{(2\pi)^3}\langle B_a(\mathbf{p}_1)B_b(\mathbf{k}-\mathbf{p}_1) \\ &\quad\times B_c(\mathbf{p}_2)B_d(\mathbf{k}+\mathbf{p}_2)\rangle \quad (4.13) \\ &= \frac{B_0^2}{8\pi^2}F(k) \quad (4.14) \end{aligned}$$

with

$$\begin{aligned} F(k) \equiv \int \frac{d^3\mathbf{p}_1}{(2\pi)^3} & f(p_1)f(|\mathbf{k}-\mathbf{p}_1|)A(\mathbf{k},-\mathbf{k};\mathbf{p}_1) \\ & \times A(\mathbf{k},-\mathbf{k};\mathbf{k}-\mathbf{p}_1), \end{aligned} \quad (4.15)$$

where

$$A(\mathbf{k}_1,\mathbf{k}_2;\mathbf{u}) = \frac{\mathbf{k}_1\cdot\mathbf{k}_2}{k_1k_2} - \frac{(\mathbf{k}_1\cdot\mathbf{u})(\mathbf{k}_2\cdot\mathbf{u})}{u^2k_1k_2}. \tag{4.16}$$

Hence, the scale dependence of the source correlator is set by the magnetic-field power spectrum $P_B(k)$ proportional to the function $f(k)$ [recall Eq. (4.3)].

3. The energy density

Collecting these results, and retaining only the logarithmically enhanced contribution from Eq. (4.12), the GW scalar-polarization power spectrum can be written as

$$P_h = \left(\frac{aH}{k}\right)^2 \frac{B_0^2}{8\pi}\frac{\ln^2(k^2\tau_R^2)}{a^8H^4}F(k). \tag{4.17}$$

This representation is particularly convenient for expressing all results in terms of energy densities, defined for a species A as

$$\Omega_A = \frac{1}{\rho_{\rm cr}}\frac{d\rho_A}{d\ln f}. \tag{4.18}$$

The energy density in the scalar polarization is related to its power spectrum through (we use the conventions of [112])

$$\Omega_{\rm GW}^{(b)} = \frac{1}{24}\left(\frac{k}{aH}\right)^2 P_h. \tag{4.19}$$

[The overall factor scaling as $k^2/(aH)^2$ is due to the fact that the GW energy depends on (conformal) time derivatives of the GW mode h_{ij} squared.] The magnetic-field energy density on large scales is given by $\Omega_B = B_0/(3H_0)$ (see, e.g., [103]). Parametrizing the scale factor during radiation domination as [103]

$$a(\tau) = H_0\sqrt{\Omega_{\rm rad}}\tau, \tag{4.20}$$

and multiplying the final result by $\Omega_{\rm rad}$ to account for the redshifting of quantities evaluated during radiation domination (RD), we obtain

$$\Omega_{\rm GW}^{(b)} = \frac{3}{128\pi^2}\frac{\Omega_B^2}{\Omega_{\rm rad}}[\ln|k\tau_R|]^2F(k). \tag{4.21}$$

The amplitude is consistent with [103], up to numerical coefficients reflecting our focus here on contributions from scalar polarizations only. Hence in a setup based on scalar tensor theory we can expect two contributions to the GW energy density $\Omega_{\rm GW}$—one contribution $\Omega_{\rm GW}^{(b)}$ due to scalar modes, see Eq. (4.21)—the other controlled by tensors, with the same overall coefficient $\Omega_B^2/\Omega_{\rm rad}$ but different numerical coefficients and distinct dependence on momentum k.

The methods developed in this preparatory section—which computed for the first time the energy density in GW scalar polarization as induced by magnetic-field source—set the stage for the computation of the three-point function, which we now turn to.

C. The gravitational wave three-point function

We now compute the three-point function of the Fourier modes of the scalar polarization of gravitational waves, Eq. (4.8), sourced at second order by the primordial magnetic field. As we learned, such three-point function can constitute a particular transparent quantity to measure, being not contaminated by spin-2 and spin-1 polarizations. The computation is conceptually similar to the two-point function studied in the previous section. However, the new and interesting result we aim to highlight is that only folded configurations in momentum space—corresponding to stationary signals in real space—lead to observable effects. See Fig. 1 for a representation of folded triangles. All other shapes of non-Gaussianity are washed out by time integrations involving highly oscillatory functions [42]. This illustrates the central role played by the stationary condition on the SGWB statistics in determining the measurability of the signal.

The computation of the tensor three-point function depends on the kind of interactions we wish to consider in the third-order action for tensor modes. As representative of modified gravity setup, we consider cubic terms involving time derivatives of h_{ij}, proportional to $\dot{h}_{ij}\dot{h}_{jk}\dot{h}_{ki}$, which can arise in theories containing Horndeski interactions and are absent in general relativity (see, e.g., [113] for a cosmological application of such terms). Passing to conformal time and to Fourier modes, and normalizing to make the quantities dimensionless, we consider the following expression for the bispectrum[11] of the scalar polarization as

$$\begin{aligned}\hat{B}_b(\mathbf{k_1},\mathbf{k_2},\mathbf{k_3}) &\equiv \frac{k_1k_2k_3}{(aH)^3}\langle h_{\mathbf{k_1}}(\tau)h_{\mathbf{k_2}}(\tau)h_{\mathbf{k_3}}(\tau)\rangle'_{\mathbf{k_1}+\mathbf{k_2}+\mathbf{k_3}=\mathbf{0}}\\ &= \frac{k_1k_2k_3}{(a^2H)^3}\mathcal{I}_{(3)}(\tau)\langle S_{\mathbf{k_1}}S_{\mathbf{k_2}}S_{\mathbf{k_3}}\rangle'_{\mathbf{k_1}+\mathbf{k_2}+\mathbf{k_3}=\mathbf{0}},\end{aligned} \tag{4.22}$$

where the prime indicates that the overall momentum-conserving δ function has been factored out, and

$$\mathcal{I}_{(3)}(\tau) \equiv \int d\tau_1 d\tau_2 d\tau_3 \frac{g_{k_1}(\tau,\tau_1)}{a(\tau_1)}\frac{g_{k_2}(\tau,\tau_2)}{a(\tau_2)}\frac{g_{k_3}(\tau,\tau_3)}{a(\tau_3)}. \tag{4.23}$$

[11]We indicate with a hat the bispectrum, to differentiate this definition with Eq. (2.8) where the three-point function for quantities without time derivatives is considered.

1. Time integral

The first main ingredient of Eq. (4.22) is the time integral of Eq. (4.23), subject to the momentum-conservation condition $\mathbf{k_1}+\mathbf{k_2}+\mathbf{k_3}=0$. As in the two-point function analysis of Sec. IV B, the integrand is highly oscillatory. However, in this case the oscillations always involve odd combinations of sine and cosine terms, such as $\cos[(k_1+k_2+k_3)\tau]$, $\cos[(k_1+k_2-k_3)\tau]$, and so on. These average to zero unless the argument of the cosine vanishes. This occurs precisely for folded triangles, e.g., when $k_3=k_1+k_2$. See Fig. 1 for a graphical representation.

For such configurations, the integral develops a logarithmic enhancement at late times. In the case $k_1+k_2=k_3$, we obtain

$$\begin{aligned}\mathcal{I}_{(3)}(\tau)&=\frac{\pi}{8k_1k_2k_3}\frac{1}{H^3a^6}\left[\ln(k_1\tau_R)\ln(k_3\tau_R)+\ln(k_2\tau_R)\ln(k_3\tau_R)-\ln(k_1\tau_R)\ln(k_2\tau_R)\right]\\&\equiv\frac{1}{k_1k_2k_3(a^2H)^3}G_2(k_1,k_2),\end{aligned}\tag{4.24}$$

where we introduced the function G_2 of k_1, k_2, $k_3=k_1+k_2$ to keep track of the log-enhanced contributions. The other two cases, $k_1+k_3=k_2$ and $k_2+k_3=k_1$, can be treated analogously.

2. Source contribution

The last coefficient in Eq. (4.22)—the source three-point function—can be obtained by carefully performing the convolution integrals. The result is

$$\begin{aligned}\langle S_{\mathbf{k_1}}S_{\mathbf{k_2}}S_{\mathbf{k_3}}\rangle'&=\frac{k_{1a}k_{1b}k_{2c}k_{2d}k_{3e}k_{3f}}{k_1^2k_2^2k_3^2}\langle B_a(\mathbf{p}_1)B_b(\mathbf{k}_1-\mathbf{p}_1)B_c(\mathbf{p}_2)B_d(\mathbf{k}_2-\mathbf{p}_2)B_e(\mathbf{p}_3)B_f(\mathbf{k}_3-\mathbf{p}_3)\rangle'\\&=2\int\frac{d^3\mathbf{p}_1}{(2\pi)^3}P_B(p_1)P_B(|\mathbf{k}_1-\mathbf{p}_1|)\{P_B(|\mathbf{k}_2+\mathbf{p}_1|)\mathcal{T}_2(\mathbf{k}_1,\mathbf{k}_2;\mathbf{p}_1)+P_B(|\mathbf{k}_3+\mathbf{p}_1|)\mathcal{T}_3(\mathbf{k}_1,\mathbf{k}_2;\mathbf{p}_1)\},\end{aligned}$$

where

$$\begin{aligned}\mathcal{T}_2(\mathbf{k}_1,\mathbf{k}_2;\mathbf{p}_1)&=A(\mathbf{k}_1,\mathbf{k}_2;\mathbf{p}_1)A(\mathbf{k}_1,\mathbf{k}_3;\mathbf{k}_1-\mathbf{p}_1)A(\mathbf{k}_2,\mathbf{k}_3;\mathbf{k}_2+\mathbf{p}_1),\\\mathcal{T}_3(\mathbf{k}_1,\mathbf{k}_2;\mathbf{p}_1)&=A(\mathbf{k}_1,\mathbf{k}_3;\mathbf{p}_1)A(\mathbf{k}_1,\mathbf{k}_2;\mathbf{k}_1-\mathbf{p}_1)A(\mathbf{k}_2,\mathbf{k}_3;\mathbf{k}_3+\mathbf{p}_1).\end{aligned}$$

The function A appearing above is defined in Eq. (4.16).

3. Folded configurations

As we learned above, the physically interesting limit is that of "folded triangles," in which the three momenta are collinear. See Fig. 1. One example is

$$\mathbf{k_1}=k_1\hat{a},\qquad\mathbf{k_2}=k_2\hat{a},\qquad\mathbf{k_3}=-k_3\hat{a},\tag{4.25}$$

with the condition $k_1+k_2=k_3$, for a certain side direction $\hat{a}$. In this case it is convenient to define

$$\mathcal{T}(\mathbf{u})\equiv1-\frac{(\hat{a}\cdot\mathbf{u})^2}{|\mathbf{u}|^2},\tag{4.26}$$

so that the source correlator reduces to

$$\begin{aligned}\langle S_{\mathbf{k_1}}S_{\mathbf{k_2}}S_{\mathbf{k_3}}\rangle'&=2B_0^3\int\frac{d^3\mathbf{p}_1}{(2\pi)^3}f(p_1)f(|\mathbf{k}_1-\mathbf{p}_1|)\{3f(|\mathbf{k}_2+\mathbf{p}_1|)\mathcal{T}(\mathbf{p}_1)\mathcal{T}(\mathbf{k}_1-\mathbf{p}_1)\mathcal{T}(\mathbf{k}_2+\mathbf{p}_1)\\&\quad+f(|\mathbf{k}_3+\mathbf{p}_1|)\mathcal{T}(\mathbf{p}_1)\mathcal{T}(\mathbf{k}_1-\mathbf{p}_1)\mathcal{T}(\mathbf{k}_3+\mathbf{p}_1)\},\\&\equiv B_0^3G_1(k_1,k_2,\hat{a})\end{aligned}$$

where the function G_1 in the last line of the previous formula depends on k_1, k_2, $k_3 = k_1 + k_2$, as well as on the direction $\hat{a}$ of the folded triangle sides in momentum space.

Substituting the results of Eqs. (4.3) and (4.24) in the definition of the bispectrum (4.22), using the expressions for Ω_B and $a(\tau)$ introduced in Sec. IV B, and multiplying the result by $\Omega_{\rm rad}$ to take into account of redshifting during RD, we obtain

$$\hat{B}_b(\mathbf{k_1}, \mathbf{k_2}, \mathbf{k_3}) = \frac{27\Omega_B^3}{\Omega_{\rm rad}^2}[G_1(k_1, k_2, \hat{a})G_2(k_1, k_2) + \text{perms}] \tag{4.27}$$

and, due to considerations above, the previous quantity has support only in the folded limit, where the momenta $\mathbf{k}_i$ are all aligned.

D. Summary of this section

Our analysis shows that cosmological magnetic fields can source a nontrivial three-point function of scalar polarizations, which, in principle, constitutes a measurable signal. Such a detection would provide a powerful probe of alternative theories of gravity predicting extra polarizations beyond the tensorial modes of general relativity.

We find that the amplitude of the GW three-point function in Eq. (4.27) scales as $\hat{B}_b \simeq \Omega_B^3/\Omega_{\rm rad}^2 \propto B_0^3\Omega_{\rm rad}$, in contrast to the magnetic-field contribution to the GW energy density, whose amplitude scales as $\Omega_{\rm GW}^{(b)} \simeq \Omega_B^2/\Omega_{\rm rad} \propto B_0^2\Omega_{\rm rad}$ [recall that B_0 is the parameter controlling the magnetic field amplitude—see Eq. (4.3)]. The bispectrum can be further enhanced by specific forms of the magnetic-field spectrum $P_B(k)$, which enters the convolution integrals and may preferentially amplify the three-point signal on certain scales relative to the power spectrum. In addition, the two- and three-point functions acquire distinct logarithmic contributions from time integrals, which in some regions of parameter space can increase non-Gaussian effects. A particularly illustrative case is provided by folded configurations, with momenta satisfying $k_1 \ll k_2, k_3$ and $k_1 + k_2 = k_3$. In this limit, the logarithmic term $\ln(k_1\tau_R)$ enhances the bispectrum amplitude relative to the logarithmic factors that govern the power spectrum. These considerations suggest that one may evade existing bounds on Ω_B derived from the GW energy density of two-point correlators discussed in Sec. IV B, while still obtaining a sizable three-point signal on selected scales. Exploring these possibilities in detail, both analytically and numerically, represents an interesting direction for future work, which we plan to pursue in forthcoming publications. Nevertheless, in order to obtain a very preliminary sense of how the results of this section might compare with those of Sec. III, one may tentatively regard the bispectrum shape derived from Eq. (4.27) as broadly comparable to the simple representative template of Eq. (3.20). Within this rough approximation, detectability would require the cubic root of the bispectrum amplitude to reach values of order $(\hat{B}_b)^{1/3} \sim 10^{-17}$. Under these assumptions, and disregarding overall numerical factors, this would suggest that magnetic-field amplitudes of at least $B_0 \sim 10^{-15}$ could be needed for the bispectrum to become observable. These estimates are only indicative, and a more refined analysis is left for future work.

A key outcome of our computation is that, due to time-averaging over rapid oscillations, only bispectrum shapes corresponding to "folded configurations"—which describe stationary processes in real space—yield nonvanishing contributions. All other configurations are suppressed: their contributions average to zero because of decorrelation effects, as first emphasized in [42].

The results of this section provide a concrete demonstration of the central role of the stationary condition for the feasibility of detecting scalar polarizations with our method. If scalar polarizations exist, they can be generated at second order in perturbations by sources as primordial magnetic fields, as examined here. They can contribute to the total GW two-point function—as studied in Sec. IV B—hence contaminating measurements of the GW energy density. More interesting to us, they can source three-point functions with support in folded limits, which if measured provide a unique footprint of modified gravity. More in general, we expect similar effects to occur in systems where amplified fluctuations—in scalar or vector sectors—source GW at second order in perturbations.

V. CONCLUSIONS

In this work we have proposed a novel method to detect scalar polarizations in the stochastic GW background, as predicted in theories beyond general relativity. Our approach is based on measuring three-point correlation functions of the GW signal. After averaging over the polarization angle—which accounts for the ambiguity in the definition of polarization tensors—we have shown that the detector response to three-point correlations vanishes for spin-2 and spin-1 modes, but remains nonvanishing for scalar modes. Therefore, the detection of a nonzero GW three-point correlator would provide direct evidence for the existence of scalar polarizations.

We derived analytical expressions for the response functions to GW three-point correlators for coincident ground-based detectors, for PTAs, and for astrometric measurements. Our analysis included the possibility of cross-correlating different observables, and we characterized the geometrical properties of the corresponding response functions. Furthermore, we constructed an optimal estimator for the GW three-point function and developed simple Fisher forecasts to assess the detectability of its amplitude with PTA experiments. As an illustration, we presented a concrete cosmological scenario in which GWs are induced at second order in a primordial magnetogenesis

setup, showing that such a mechanism can, in principle, generate a sizable three-point signal.

Future work will involve refining and extending the early-Universe model we introduced, as well as applying our formalism to current and forthcoming GW datasets. This will allow us to place explicit bounds on the amplitude of GW three-point correlations and, crucially, to constrain or discover the presence of scalar polarizations in the GW background.

ACKNOWLEDGMENTS

It is a pleasure to thank Ameek Malhotra for discussions. We are partially funded by the STFC Grants No. ST/T000813/1 and No. ST/X000648/1.

DATA AVAILABILITY

The data are not publicly available. The data are available from the authors upon reasonable request.

[1] M. Maggiore, *Gravitational Waves. Vol. 1: Theory and Experiments* (Oxford University Press, New York, 2007).
[2] M. Maggiore, *Gravitational Waves. Vol. 2: Astrophysics and Cosmology* (Oxford University Press, New York, 2018).
[3] N. Andersson, *Gravitational-Wave Astronomy*, Oxford Graduate Texts (Oxford University Press, New York, 2019).
[4] D. M. Eardley, D. L. Lee, and A. P. Lightman, Gravitational-wave observations as a tool for testing relativistic gravity, Phys. Rev. D **8**, 3308 (1973).
[5] D. M. Eardley, D. L. Lee, A. P. Lightman, R. V. Wagoner, and C. M. Will, Gravitational-wave observations as a tool for testing relativistic gravity, Phys. Rev. Lett. **30**, 884 (1973).
[6] C. M. Will, *Theory and Experiment in Gravitational Physics* (Cambridge University Press, Cambridge, England, 2018).
[7] T. Regimbau, The astrophysical gravitational wave stochastic background, Res. Astron. Astrophys. **11**, 369 (2011).
[8] J. D. Romano and N. J. Cornish, Detection methods for stochastic gravitational-wave backgrounds: A unified treatment, Living Rev. Relativity **20**, 2 (2017).
[9] C. Caprini and D. G. Figueroa, Cosmological backgrounds of gravitational waves, Classical Quantum Gravity **35**, 163001 (2018).
[10] G. Agazie *et al.* (NANOGrav Collaboration), The NANOGrav 15 yr data set: Evidence for a gravitational-wave background, Astrophys. J. Lett. **951**, L8 (2023).
[11] D. J. Reardon *et al.*, Search for an isotropic gravitational-wave background with the parkes pulsar timing array, Astrophys. J. Lett. **951**, L6 (2023).
[12] H. Xu *et al.*, Searching for the nano-hertz stochastic gravitational wave background with the Chinese pulsar timing array data release I, Res. Astron. Astrophys. **23**, 075024 (2023).
[13] J. Antoniadis *et al.* (EPTA and InPTA Collaborations), The second data release from the European Pulsar Timing Array—III. Search for gravitational wave signals, Astron. Astrophys. **678**, A50 (2023).
[14] B. P. Abbott *et al.* (LIGO Scientific and Virgo Collaborations), Search for tensor, vector, and scalar polarizations in the stochastic gravitational-wave background, Phys. Rev. Lett. **120**, 201102 (2018).
[15] K. J. Lee, F. A. Jenet, and R. H. Price, Pulsar timing as a probe of non-Einsteinian polarizations of gravitational waves, Astrophys. J. **685**, 1304 (2008).
[16] S. J. Chamberlin and X. Siemens, Stochastic backgrounds in alternative theories of gravity: Overlap reduction functions for pulsar timing arrays, Phys. Rev. D **85**, 082001 (2012).
[17] N. Yunes and X. Siemens, Gravitational-wave tests of general relativity with ground-based detectors and pulsar-timing arrays, Living Rev. Relativity **16**, 1 (2013).
[18] J. R. Gair, M. Vallisneri, S. L. Larson, and J. G. Baker, Testing general relativity with low-frequency, space-based gravitational-wave detectors, Living Rev. Relativity **16**, 1 (2013).
[19] J. R. Gair, J. D. Romano, and S. R. Taylor, Mapping gravitational-wave backgrounds of arbitrary polarisation using pulsar timing arrays, Phys. Rev. D **92**, 102003 (2015).
[20] N. J. Cornish, L. O'Beirne, S. R. Taylor, and N. Yunes, Constraining alternative theories of gravity using pulsar timing arrays, Phys. Rev. Lett. **120**, 181101 (2018).
[21] Z. Arzoumanian, P. T. Baker, H. Blumer, B. Becsy, A. Brazier, P. R. Brook, S. Burke-Spolaor, M. Charisi, S. Chatterjee, S. Chen *et al.*, The nanograv 12.5-year data set: Search for non-Einsteinian polarization modes in the gravitational-wave background, Astrophys. J. Lett. **923**, L22 (2021).
[22] G. Agazie, A. Anumarlapudi, A. M. Archibald, Z. Arzoumanian, J. Baier, P. T. Baker, B. Bécsy, L. Blecha, A. Brazier, P. R. Brook *et al.*, The nanograv 15 yr data set: Search for transverse polarization modes in the gravitational-wave background, Astrophys. J. Lett. **964**, L14 (2024).
[23] Z.-C. Chen, Y.-M. Wu, Y.-C. Bi, and Q.-G. Huang, Search for nontensorial gravitational-wave backgrounds in the nanograv 15-year dataset, Phys. Rev. D **109**, 084045 (2024).
[24] Y.-M. Wu, Z.-C. Chen, and Q.-G. Huang, Constraining the polarization of gravitational waves with the parkes pulsar timing array second data release, Astrophys. J. **925**, 37 (2022).

[25] N. J. Cornish, L. O'Beirne, S. R. Taylor, and N. Yunes, Constraining alternative theories of gravity using pulsar timing arrays, Phys. Rev. Lett. **120**, 181101 (2018).
[26] Y. Gong and S. Hou, The polarizations of gravitational waves, 2018, https://inspirehep.net/literature/1677329.
[27] D. P. Mihaylov, C. J. Moore, J. R. Gair, A. Lasenby, and G. Gilmore, Astrometric effects of gravitational wave backgrounds with non-Einsteinian polarizations, Phys. Rev. D **97**, 124058 (2018).
[28] L. O'Beirne and N. J. Cornish, Constraining the polarization content of gravitational waves with astrometry, Phys. Rev. D **98**, 024020 (2018).
[29] R. C. Bernardo and K.-W. Ng, Beyond the Hellings–Downs curve: Non-Einsteinian gravitational waves in pulsar timing array correlations, Astron. Astrophys. **691**, A126 (2024).
[30] Q. Liang, M.-X. Lin, and M. Trodden, A test of gravity with pulsar timing arrays, J. Cosmol. Astropart. Phys. 11 (2023) 042.
[31] Z.-C. Chen, Y.-M. Wu, Y.-C. Bi, and Q.-G. Huang, Search for nontensorial gravitational-wave backgrounds in the NANOGrav 15-year dataset, Phys. Rev. D **109**, 084045 (2024).
[32] G. Agazie *et al.* (NANOGrav Collaboration), The NANOGrav 15 yr data set: Search for transverse polarization modes in the gravitational-wave background, Astrophys. J. Lett. **964**, L14 (2024).
[33] G. Agazie *et al.*, The NANOGrav 15 yr data set: Harmonic analysis of the pulsar angular correlations, Astrophys. J. **985**, 99 (2025).
[34] E. Babichev and C. Deffayet, An introduction to the Vainshtein mechanism, Classical Quantum Gravity **30**, 184001 (2013).
[35] A. Joyce, B. Jain, J. Khoury, and M. Trodden, Beyond the cosmological standard model, Phys. Rep. **568**, 1 (2015).
[36] C. Burrage and J. Sakstein, Tests of chameleon gravity, Living Rev. Relativity **21**, 1 (2018).
[37] E. Belgacem, F. Iacovelli, M. Maggiore, M. Mancarella, and N. Muttoni, The spectral density of astrophysical stochastic backgrounds, J. Cosmol. Astropart. Phys. 04 (2025) 032.
[38] C. Powell and G. Tasinato, Probing a stationary non-Gaussian background of stochastic gravitational waves with pulsar timing arrays, J. Cosmol. Astropart. Phys. 01 (2020) 017.
[39] N. Bartolo, D. Bertacca, S. Matarrese, M. Peloso, A. Ricciardone, A. Riotto, and G. Tasinato, Anisotropies and non-Gaussianity of the cosmological gravitational wave background, Phys. Rev. D **100**, 121501 (2019).
[40] N. Bartolo, D. Bertacca, S. Matarrese, M. Peloso, A. Ricciardone, A. Riotto, and G. Tasinato, Characterizing the cosmological gravitational wave background: Anisotropies and non-Gaussianity, Phys. Rev. D **102**, 023527 (2020).
[41] B. Allen and A. C. Ottewill, Detection of anisotropies in the gravitational wave stochastic background, Phys. Rev. D **56**, 545 (1997).
[42] N. Bartolo, V. De Luca, G. Franciolini, M. Peloso, D. Racco, and A. Riotto, Testing primordial black holes as dark matter with LISA, Phys. Rev. D **99**, 103521 (2019).
[43] S. Drasco and E. E. Flanagan, Detection methods for nonGaussian gravitational wave stochastic backgrounds, Phys. Rev. D **67**, 082003 (2003).
[44] Y. Himemoto, A. Taruya, H. Kudoh, and T. Hiramatsu, Detecting a stochastic background of gravitational waves in the presence of non-Gaussian noise: A Performance of generalized cross-correlation statistic, Phys. Rev. D **75**, 022003 (2007).
[45] N. Seto, Non-Gaussianity analysis of GW background made by short-duration burst signals, Phys. Rev. D **80**, 043003 (2009).
[46] L. Martellini and T. Regimbau, Semiparametric approach to the detection of non-Gaussian gravitational wave stochastic backgrounds, Phys. Rev. D **89**, 124009 (2014).
[47] M. Tsuneto, A. Ito, T. Noumi, and J. Soda, Searching for bispectrum of stochastic gravitational waves with pulsar timing arrays, J. Cosmol. Astropart. Phys. 03 (2019) 032.
[48] R. Buscicchio, A. Ain, M. Ballelli, G. Cella, and B. Patricelli, Detecting non-Gaussian gravitational wave backgrounds: A unified framework, Phys. Rev. D **107**, 063027 (2023).
[49] M. Ballelli, R. Buscicchio, B. Patricelli, A. Ain, and G. Cella, Improved detection statistics for non-Gaussian gravitational wave stochastic backgrounds, Phys. Rev. D **107**, 124044 (2023).
[50] P. Adshead and E. A. Lim, 3-pt statistics of cosmological stochastic gravitational waves, Phys. Rev. D **82**, 024023 (2010).
[51] E. Dimastrogiovanni, M. Fasiello, and G. Tasinato, Searching for Fossil fields in the gravity sector, Phys. Rev. Lett. **124**, 061302 (2020).
[52] A. Ricciardone and G. Tasinato, Anisotropic tensor power spectrum at interferometer scales induced by tensor squeezed non-Gaussianity, J. Cosmol. Astropart. Phys. 02 (2018) 011.
[53] N. Bartolo, V. Domcke, D. G. Figueroa, J. García-Bellido, M. Peloso, M. Pieroni, A. Ricciardone, M. Sakellariadou, L. Sorbo, and G. Tasinato, Probing non-Gaussian stochastic gravitational wave backgrounds with LISA, J. Cosmol. Astropart. Phys. 11 (2018) 034.
[54] B. Allen and J. D. Romano, Detecting a stochastic background of gravitational radiation: Signal processing strategies and sensitivities, Phys. Rev. D **59**, 102001 (1999).
[55] A. Abac *et al.*, The science of the Einstein telescope, arXiv:2503.12263.
[56] R. w. Hellings and G. s. Downs, Upper limits on the isotropic gravitational radiation background from pulsar timing analysis, Astrophys. J. Lett. **265**, L39 (1983).
[57] R. Fakir, Gravity wave watching, Astrophys. J. **426**, 74 (1994).
[58] T. Pyne, C. R. Gwinn, M. Birkinshaw, T. M. Eubanks, and D. N. Matsakis, Gravitational radiation and very long baseline interferometry, Astrophys. J. **465**, 566 (1996).
[59] N. Kaiser and A. H. Jaffe, Bending of light by gravity waves, Astrophys. J. **484**, 545 (1997).
[60] A. H. Jaffe, Observing gravitational radiation with QSO proper motions and the SKA, New Astron. Rev. **48**, 1483 (2004).

[61] L. G. Book and E. E. Flanagan, Astrometric effects of a stochastic gravitational wave background, Phys. Rev. D **83**, 024024 (2011).
[62] L. Shao *et al.*, Testing gravity with pulsars in the SKA era, Proc. Sci., AASKA14 (**2015**) 042 [arXiv:1501.00058].
[63] T. Prusti *et al.* (Gaia Collaboration), The Gaia mission, Astron. Astrophys. **595**, A1 (2016).
[64] C. J. Moore, D. P. Mihaylov, A. Lasenby, and G. Gilmore, Astrometric search method for individually resolvable gravitational wave sources with Gaia, Phys. Rev. Lett. **119**, 261102 (2017).
[65] S. A. Klioner, Gaia-like astrometry and gravitational waves, Classical Quantum Gravity **35**, 045005 (2018).
[66] C. Boehm *et al.* (Theia Collaboration), Theia: Faint objects in motion or the new astrometry frontier, arXiv:1707.01348.
[67] W. Qin, K. K. Boddy, M. Kamionkowski, and L. Dai, Pulsar-timing arrays, astrometry, and gravitational waves, Phys. Rev. D **99**, 063002 (2019).
[68] J. Garcia-Bellido, H. Murayama, and G. White, Exploring the early Universe with Gaia and Theia, J. Cosmol. Astropart. Phys. 12 (2021) 023.
[69] F. Malbet *et al.*, Theia: Science cases and mission profiles for high precision astrometry in the future, in *SPIE Astronomical Telescopes + Instrumentation 2022: Optical, Infrared, and Millimeter Wave* (2022); arXiv:2207.12540.
[70] J. Darling, A. E. Truebenbach, and J. Paine, Astrometric limits on the stochastic gravitational wave background, Astrophys. J. **861**, 113 (2018).
[71] Y. Wang, K. Pardo, T.-C. Chang, and O. Doré, Constraining the stochastic gravitational wave background with photometric surveys, Phys. Rev. D **106**, 084006 (2022).
[72] Y. Wang, K. Pardo, T.-C. Chang, and O. Doré, Gravitational wave detection with photometric surveys, Phys. Rev. D **103**, 084007 (2021).
[73] M. Çalışkan, Y. Chen, L. Dai, N. Anil Kumar, I. Stomberg, and X. Xue, Dissecting the stochastic gravitational wave background with astrometry, J. Cosmol. Astropart. Phys. 05 (2024) 030.
[74] K. Pardo, T.-C. Chang, O. Doré, and Y. Wang, Gravitational wave detection with relative astrometry using Roman's galactic bulge time domain survey, arXiv:2306.14968.
[75] S. Jaraba, J. García-Bellido, S. Kuroyanagi, S. Ferraiuolo, and M. Braglia, Stochastic gravitational wave background constraints from Gaia DR3 astrometry, Mon. Not. R. Astron. Soc. **524**, 3609 (2023).
[76] J. Darling, A new approach to the low-frequency stochastic gravitational-wave background: Constraints from quasars and the astrometric Hellings–Downs curve, Astrophys. J. Lett. **982**, L46 (2025).
[77] S. Aoyama, D. Yamauchi, M. Shiraishi, and M. Ouchi, Gaia 400,894 QSO constraint on the energy density of low-frequency gravitational waves, arXiv:2105.04039.
[78] G. Mentasti and C. R. Contaldi, Observing gravitational waves with solar system astrometry, J. Cosmol. Astropart. Phys. 05 (2024) 028.
[79] K. Inomata, M. Kamionkowski, C. M. Toral, and S. R. Taylor, Overlap reduction functions for pulsar timing arrays and astrometry, Phys. Rev. D **110**, 063547 (2024).
[80] N. M. J. Cruz, A. Malhotra, G. Tasinato, and I. Zavala, Astrometry meets pulsar timing arrays: Synergies for gravitational wave detection, Phys. Rev. D **112**, 083558 (2025).
[81] M. Vaglio, M. Falxa, G. Mentasti, A. I. Renzini, A. Kuntz, E. Barausse, C. Contaldi, and A. Sesana, Searching for gravitational waves with Gaia and its cross-correlation with PTA: Absolute vs relative astrometry, arXiv:2507.18593.
[82] S. Ghonge, J. Brandt, J. M. Sullivan, M. Millhouse, K. Chatziioannou, J. A. Clark, T. Littenberg, N. Cornish, S. Hourihane, and L. Cadonati, Assessing and mitigating the impact of glitches on gravitational-wave parameter estimation: A model agnostic approach, Phys. Rev. D **110**, 122002 (2024).
[83] N. Karnesis, A. Sasli, R. Buscicchio, and N. Stergioulas, Characterization of non-Gaussian stochastic signals with heavier-tailed likelihoods, Phys. Rev. D **111**, 022005 (2025).
[84] X. Xue, Z. Pan, and L. Dai, Non-Gaussian statistics of nanohertz stochastic gravitational waves, Phys. Rev. D **111**, 043022 (2025).
[85] R. C. Bernardo, S. Appleby, and K.-W. Ng, Toward a test of Gaussianity of a gravitational wave background, J. Cosmol. Astropart. Phys. 01 (2025) 017.
[86] M. Falxa and A. Sesana, Modeling non-Gaussianities in pulsar timing array data analysis using Gaussian mixture models, arXiv:2508.08365.
[87] M. Anholm, S. Ballmer, J. D. E. Creighton, L. R. Price, and X. Siemens, Optimal strategies for gravitational wave stochastic background searches in pulsar timing data, Phys. Rev. D **79**, 084030 (2009).
[88] Y. Ali-Haïmoud, T. L. Smith, and C. M. F. Mingarelli, Fisher formalism for anisotropic gravitational-wave background searches with pulsar timing arrays, Phys. Rev. D **102**, 122005 (2020).
[89] Y. Ali-Haïmoud, T. L. Smith, and C. M. F. Mingarelli, Insights into searches for anisotropies in the nanohertz gravitational-wave background, Phys. Rev. D **103**, 042009 (2021).
[90] N. M. J. Cruz, A. Malhotra, G. Tasinato, and I. Zavala, Measuring kinematic anisotropies with pulsar timing arrays, Phys. Rev. D **110**, 063526 (2024).
[91] N. M. J. Cruz, A. Malhotra, G. Tasinato, and I. Zavala, Measuring the circular polarization of gravitational waves with pulsar timing arrays, Phys. Rev. D **110**, 103505 (2024).
[92] G. Agazie *et al.* (NANOGrav Collaboration), The NANOGrav 15 yr data set: Detector characterization and noise budget, Astrophys. J. Lett. **951**, L10 (2023).
[93] A. Lewis, GetDist: A Python package for analysing Monte Carlo samples, J. Cosmol. Astropart. Phys. 08 (2025) 025.
[94] J. Ellis, M. Fairbairn, G. Franciolini, G. Hütsi, A. Iovino, M. Lewicki, M. Raidal, J. Urrutia, V. Vaskonen, and H. Veermäe, What is the source of the PTA GW signal?, Phys. Rev. D **109**, 023522 (2024).
[95] D. G. Figueroa, M. Pieroni, A. Ricciardone, and P. Simakachorn, Cosmological background interpretation of pulsar timing array data, Phys. Rev. Lett. **132**, 171002 (2024).

[96] D. Liang, S. Chen, C. Zhang, and L. Shao, Unveiling the existence of nontensorial gravitational-wave polarizations from individual supermassive black hole binaries with pulsar timing arrays, Phys. Rev. D **110**, 084040 (2024).
[97] A. A. Kugarajh, M. Traforetti, A. Maselli, S. Matarrese, and A. Ricciardone, Scalar-induced gravitational waves in modified gravity, arXiv:2502.20137.
[98] R. Durrer and A. Neronov, Cosmological magnetic fields: Their generation, evolution and observation, Astron. Astrophys. Rev. **21**, 62 (2013).
[99] G. Domènech, Scalar induced gravitational waves review, Universe **7**, 398 (2021).
[100] J. E. Gammal *et al.* (LISA Cosmology Working Group), Reconstructing primordial curvature perturbations via scalar-induced gravitational waves with LISA, J. Cosmol. Astropart. Phys. 05 (2025) 062.
[101] A. Ghaleb, A. Malhotra, G. Tasinato, and I. Zavala, Bayesian reconstruction of primordial perturbations from induced gravitational waves, Phys. Rev. D **112**, 123538 (2025).
[102] R. Durrer, P. G. Ferreira, and T. Kahniashvili, Tensor microwave anisotropies from a stochastic magnetic field, Phys. Rev. D **61**, 043001 (2000).
[103] C. Caprini and R. Durrer, Gravitational wave production: A strong constraint on primordial magnetic fields, Phys. Rev. D **65**, 023517 (2001).
[104] A. Mack, T. Kahniashvili, and A. Kosowsky, Microwave background signatures of a primordial stochastic magnetic field, Phys. Rev. D **65**, 123004 (2002).
[105] L. Pogosian, T. Vachaspati, and S. Winitzki, Signatures of kinetic and magnetic helicity in the CMBR, Phys. Rev. D **65**, 083502 (2002).
[106] C. Caprini, R. Durrer, and T. Kahniashvili, The cosmic microwave background and helical magnetic fields: The Tensor mode, Phys. Rev. D **69**, 063006 (2004).
[107] J. R. Shaw and A. Lewis, Massive neutrinos and magnetic fields in the early Universe, Phys. Rev. D **81**, 043517 (2010).
[108] S. Saga, H. Tashiro, and S. Yokoyama, Limits on primordial magnetic fields from direct detection experiments of gravitational wave background, Phys. Rev. D **98**, 083518 (2018).
[109] A. Bhaumik, T. Papanikolaou, and A. Ghoshal, Vector induced gravitational waves sourced by primordial magnetic fields, J. Cosmol. Astropart. Phys. 08 (2025) 054.
[110] S. Maiti, D. Maity, and R. Srikanth, Probing reheating phase via non-helical magnetogenesis and secondary gravitational waves, Phys. Rev. D **112**, 063552 (2025).
[111] B. Atkins, D. Chowdhury, A. Marriott-Best, and G. Tasinato, Inflationary magnetogenesis beyond slow-roll and its induced gravitational waves, Phys. Rev. D **112**, 063534 (2025).
[112] K. Kohri and T. Terada, Semianalytic calculation of gravitational wave spectrum nonlinearly induced from primordial curvature perturbations, Phys. Rev. D **97**, 123532 (2018).
[113] O. Ozsoy, M. Mylova, S. Parameswaran, C. Powell, G. Tasinato, and I. Zavala, Squeezed tensor non-Gaussianity in non-attractor inflation, J. Cosmol. Astropart. Phys. 09 (2019) 036.